Topological defects in Ring-Coupled Condensates

Nickolas Theodoulou
Supervisor: Dr Anna Posazhennikova

March 26, 2019

Abstract

A system of ring-coupled condensates is considered in-which the dynamics of the system will be studied. The coupled Gross-Pitanaevskii Equations that describe the dynamics of the system in terms of the population imbalance and a phase difference are derived. Firstly, a double-well potential is considered. An an-harmonic generalization is then used to discuss the Josephson effect and plasma oscillations. A non-linear regime analogy of a pendulum is used to better understand the physics of these systems. Λ and the initial conditions completely govern the properties of the Josephson tunneling in a symmetric potential. For $\Lambda < \lambda_c$, where λ_c is a critical value, sinusoidal oscillations are found to occur. At λ_c, the oscillations become an-harmonic. The energy difference ΔE in the asymmetric potential is found to produce a running phase without self-trapping occurring under the right conditions. Macroscopic quantum self-trapping occurs in the asymmetric potential when the parameter Λ exceeds a crossover value defined as $\Lambda_s = 1/\sqrt{1 - z(0)^2}$. Triple well systems were also investigated and similar oscillations were also found.

Contents

I Introduction

A Bose-Einstein condensate (BEC) is a state of matter that occurs when $T \to 0$ for a system of bosons. This typically occurs in systems of cold atoms. In this regime, the system can be described by a non-linear Schrödinger equation known as the Gross-Pitvaeskii equation (GPE) [1, 2]. The GPE is a central equation to this project.

A BEC was first predicted in 1925 due to the correspondence between Bose and Einstein. A paper in which Plank's law was derived without reference to classical physics was sent by Bose to Einstein. This paper was translated in 1924 by Einstein and published as Ref. [3]. Einstein built upon this work in two papers by describing what is known today as a Bose gas. A bose gas is governed by Bose-Einstein statistics that describe the behaviour of integer spin particles (bosons). Einstein also noticed a peculiar feature of the distribution of the atoms predicted by the statistics. At a very low but finite temperature, a large fraction of the atoms would occupy the ground state energy. The condition for this to occur is the de Broglie wavelength, λ_{dB}, of each atom must be large enough to overlap with neighbouring atoms. More precisely, $n\lambda_{\mathrm{dB}}^3 > 2.61$, where n is the particle density.

This prediction was not further pursued until Bose-Einstein condensation was considered a possible mechanism underlying super-fluidity in liquid helium 4 in a paper published by London Ref. [4]. Some consequences of this were then discussed by Tisza in Ref. [5].Bose-Einstein condensation was observed in 1995. Davis et al. observed the phenomena in sodium and published their results in Ref. [6]. Anderson et al. published Ref. [7] in which a vapor of rubidium-87 atoms were produced. The atoms were confined by magnetic fields with the condensate first appearing at a temperature of 170 nK and number density of $2.5 \times 10^{12}\,\mathrm{cm}^{-3}$ and was preserved for 15 seconds. A sharp peak in the velocity distribution is a clear indication of a BEC, this can be seen in Fig.1.

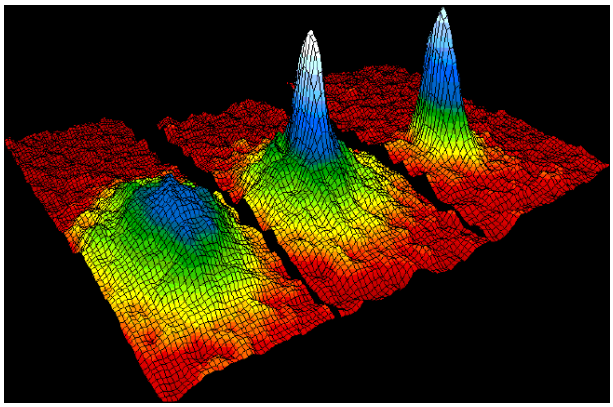

Figure 1: The velocity distribution of rubidium atoms from the experiment conducted in Ref. [7]. The left frame corresponds to gas just above condensation; the middle, after the appearance of the condensate; the right, further evaporation leaving behind a sample of a nearly pure condensate. The field of view is 200 µm by 200 µm and corresponds to the distance moved in 0.05 s. The colour is a spectrum of the number of atoms at each velocity. The red corresponds to fewer atoms at a given velocity with white corresponding to the most atoms at a given velocity.

A. Magneto-Optical Trap

A typical way to observe Bose-Einstein condensation in a lab is to use a magneto-optical trap (MOT). The exact details of how an MOT cools a real atom in three dimensions is somewhat complex however the basic principle of how it works will be discussed. A laser is applied to a sample such that it is cooled from six sides of the apparatus. This leads to momentum being transferred from the sample to photons scattering off an atom which can be thought of as a radiation-pressure force. If it is a strong atomic transition that is excited, it is possible to scatter more than 10^7 photons per second which produces large accelerations up to $10^4 g$. The radiation-pressure force is controlled in such a way that the atoms are brought to a velocity near zero (cooled) at a particular point in space (trapping). The cooling is possible due to the Doppler effect. The photons are scattered at a higher rate if the laser frequency is below the atomic resonance frequency of the atom if the atom is moving along the direction of the laser beam compared to if it is moving against the direction of the laser

beam. This means a larger force is applied to the counter-propagating atoms. As lasers are applied from all 6 directions, only the velocity-dependent force is applied to the atoms which opposes the motion of the atoms. This is what provides a strong damping of atomic motion.

The atoms will diffuse out of the region if no position dependence is applied by the radiation-pressure force. Hence, an in-homogeneous magnetic field is applied to the trapping region. Due to Zeeman shifts, the magnetic field is what determines the rate at which an atom in a particular position scatters photons from all the beams causing the atoms to be pushed to a particular point in space. This greatly increases the atomic density and a Bose-gas will condensate to a BEC.

Alkali atoms are well suited for an MOT as they have an internal energy-level structure that is favourable for cooling to low temperatures. Through careful calibration, it is possible to create a system where two BEC's are in a close enough proximity to allow the so-called Josephson tunneling through the laser barrier between them. A suitable framework to study this theoretically is Gross-Pitaevskii theory which will be discussed in theory in Sec.II and is central to this investigation.

B. Jospehson Junction

The Josephson effect is the phenomenon of a current between two coherent states that flows indefinitely without a voltage being applied. This occurs across a device known as a Josephson junction which consists of a non-superconducting material sandwiched between two layers of superconducting material. Pairs of superconducting electrons were first predicted to be able to tunnel through the non-superconducting barrier in Ref. [8]. The author later won the Nobel prize in physics in 1973. In the case if weakly linked BECs, it is common for oscillations to be observed when particles tunnel between two superconducting regions. Josephson-type effect will later be highlighted and discussed throughout Sec.III.

C. Outline

The main aim of the work conducted is to study in detail the tunneling effect between BECs. The BEC systems modeled include a double well symmetric trap and asymmetric trap, where terms that are typically neglected in other literature will be considered. A triple well system will also be studied. The paper is structured in the following way:

In Sec.II, the theoretical framework for a double well system is introduced within which the GPE is derived. This is a central equation that will be solved for both a double well and triple well system. The ground state energy of a non-interacting Bose gas is also discussed and mean-field theory is briefly highlighted as it is used to include interactions. The equations of motion of the double well Bose-Einstein condensate are derived using the GPE for both the symmetric and asymmetric case.

In Sec.III, the dynamic behaviour of the symmetric double well is investigated. The dynamics of the non-linear regime are investigated by changing various parameters and the initial conditions of the equations. Macroscopic quantum self trapping is also observed and discussed. A phase portrait is also plotted showing interesting solutions that arise from the momentum dependence of the potential energy. In Sec.IIII., an asymmetric double well is considered and a new regime is found for a large energy gap. In Sec.IIIK., some of the previously ignored terms in the GPE are discussed which are found to make the symmetric well an-harmonic.

In Sec.IV, a triple well BEC is studied. The equations of motion for the system are derived and plotted for various parameters.

In Sec.V, the main results are summarized and conclusions are drawn. Ideas on how the work conducted could be extended. Other more complex systems will also be discussed.

Appendices(A-E) are included as they go into more detail about how certain relations are derived. The final results of the Appendices are included in the main text such that the reader has the freedom to choose whether to read the appendices along with the main text. Appendix.F gives an example of the Runge-Kutta code used to solve the coupled differential equations.

II Theoretical Framework

A central equation to Bose-Einstein condensation is the GPE. In this section the GPE will be derived. It will later be solved to find the coupled equations describing a symmetric double well. These coupled equations are then later solved in Sec.III to better understand various systems such as the symmetric double well trap.

A. Derivation of the GrossPitaevskii Equation

The many body Hamiltonian that describes interacting bosons confined by an external potential V_{ext} is given by

$$\hat{H} = \int d\mathbf{r}\, \hat{\Psi}^\dagger(\mathbf{r}) \Big[-\frac{\hbar^2}{2m}\nabla^2 + V_{\text{ext}}(\mathbf{r}) \Big] \hat{\Psi}(\mathbf{r}) + \frac{1}{2}\int d\mathbf{r} d\mathbf{r}'\, \hat{\Psi}^\dagger(\mathbf{r})\, \hat{\Psi}^\dagger(\mathbf{r}') \mathbf{V}(\mathbf{r}-\mathbf{r}')\, \hat{\Psi}(\mathbf{r}')\, \hat{\Psi}(\mathbf{r}), \tag{1}$$

where $\hat{\Psi}(\mathbf{r})$ and $\hat{\Psi}^\dagger(\mathbf{r})$ are the boson field operators that annihilate and create a particle at the position $\mathbf{r}$, respectively, and $V_{\text{ext}}(\mathbf{r})$ is the two-body inter-atomic potential [9]. Where the other symbols are defined as ∇ being the differential operator and m the mass of the boson. Typically, mean-field approaches are developed for interacting systems due to the impracticability of solving many-body Schrödinger equations. They also make it possible to understand the behavior of a system in terms of a set of parameters that have a clear physical meaning as well as avoiding heavy numerical work. The basic idea for a mean-field description of a dilute Bose gas was first by Bogolubov in Ref. [10]. The important concept that should be taken from the paper is to separate out the condensate contribution to the bosonic field operator. Generally, the field operators are written as $\hat{\Psi}(\mathbf{r}) = \sum_\alpha \Psi_\alpha(\mathbf{r})\hat{a}_\alpha$ where $\Psi_\alpha(\mathbf{r})$ are the single-particle wave functions and $\hat{a}_\alpha$ is the corresponding annihilation operator which is defined in Fock space. The creation and annihilation operators $\hat{a}^\dagger_\alpha$ and $\hat{a}_\alpha$ for Bosons are defined as

$$\hat{a}^\dagger_\alpha \left|n_0, n_1, ..., n_\alpha, ...\right\rangle = \sqrt{n_\alpha + 1}\left|n_0, n_1, ..., n_{\alpha+1}, ...\right\rangle, \tag{2}$$

$$\hat{a}_\alpha \left|n_0, n_1, ..., n_\alpha, ...\right\rangle = \sqrt{n_\alpha}\left|n_0, n_1, ..., n_{\alpha-1}, ...\right\rangle, \tag{3}$$

where $n_\alpha$is the number operator, $\hat{n}_\alpha = \hat{a}^\dagger_\alpha \hat{a}_\alpha$, giving the number of atoms in the single-particle α-state.

From the framework, it is important to note that Bose-Einstein condensation occurs when n_0 (the number of atoms of a particular single-particle state) becomes very large such that $n_0 \gg 1$ and the ratio n_0/N remains finite in the thermodynamic limit $N \to \infty$. This is because in this limit, $n_0 \pm 1 \simeq n_0$. Therefore, the states n_0 and n_0+1 correspond to the same physical configuration and the operators can be approximated to $a_0 = a^\dagger_\alpha = \sqrt{n_0}$. When BEC occurs for a uniform gas in a volume V in the single particle state $\psi_0 = 1/\sqrt{V}$ has zero momentum meaning the field operator $\hat{\Psi}(\mathbf{r})$ can be written as $\hat{\Psi}(\mathbf{r}) = \sqrt{n_0/V} + \Psi'(\mathbf{r})$. As $\Psi'(\mathbf{r})$ can be treated as a small perturbation, Bogoliubov developed the "first order theory" for the excitations of interacting Bose gases. The generalization to the case of nonuniform and time dependent configurations is given as

$$\hat{\Psi}(\mathbf{r}, t) = \Phi(\mathbf{r}, t) + \Psi'(\mathbf{r}, t), \tag{4}$$

where the Heisenberg representation for the field operators have been used. $\Phi(\mathbf{r}, t)$ is a complex function defined as the expectation value of the field operator given as

$$\Phi(\mathbf{r}, t) \equiv \langle \Psi'(\mathbf{r}, t) \rangle. \tag{5}$$

Eq.(4) is particularly useful when $\Psi'(\mathbf{r}, t)$ is small as the depletion of the condensate is also small. The wave function of the condensate, $\Phi(\mathbf{r}, t)$, can be derived using the time evolution of the field operator, $\hat{\Psi}(\mathbf{r}, t)$, along with the Heisenberg equation by substituting in the Hamiltonian Eq.(1). This gives

$$i\hbar\frac{\partial}{\partial t}\hat{\Psi}(\mathbf{r}, t) = [\hat{\Psi}, \hat{H}] = \Big[-\frac{\hbar^2}{2m}\nabla^2 + V_{\text{ext}}(\mathbf{r}) + \int d\mathbf{r}' \hat{\Psi}^\dagger(\mathbf{r}', t)\mathbf{V}(\mathbf{r}-\mathbf{r}')\hat{\Psi}(\mathbf{r}', t) \Big] \hat{\Psi}(\mathbf{r}, t). \tag{6}$$

The step by step procedure of solving Eq.(6) is included in Appendix A. This leads to the GrossPitaevskii Equation defined as

$$i\hbar\frac{\partial}{\partial t}\Phi(\mathbf{r}, t) = \Big(-\frac{\hbar^2}{2m}\nabla^2 + V_{\text{ext}}(\mathbf{r}) + g|\Phi(\mathbf{r}, t)|^2 \Big) \Phi(\mathbf{r}, t). \tag{7}$$

It is important to note that the equation is only valid when the S-wave scattering length is much smaller than the average distance between atoms and $N \gg 1$, where N is the number of atoms in the condensate. The appearance of the narrow peak of the condensate in both coordinate and momentum space is an interesting feature of a trapped Bose gas that has significant consequences in both experimental and theoretical analysis.

B. Ground State Energy of a Condensate of Non-Interacting Bosons

In the case of non−interacting ($g = 0$) alkali atoms, the GPE is of the form of a 3D harmonic oscillator where the external potential $V_{\rm ext}$ is defined as

$$V_{\rm ext} = \frac{m}{2}(\omega_x^2 x^2 + \omega_y^2 y^2 + \omega_z^2 z^2). \tag{8}$$

In this configuration, the particles are treated as point-like. If the atom-atom interaction is ignored then the many-body Hamiltonian for the system is the sum of the single-particle Hamiltonian with the eigenvalues given by

$$\epsilon_{n_x n_y n_z} = \left(n_x + \frac{1}{2}\hbar\omega_x\right) + \left(n_y + \frac{1}{2}\hbar\omega_y\right) + \left(n_z + \frac{1}{2}\hbar\omega_z\right), \tag{9}$$

where n_x, n_y and n_z are non-negative integers.

The ground state $\phi(\mathbf{r_1}, ..., \mathbf{r}_N)$ of this system with N non-interacting bosons confined in the potential (8) is determined when all the particles are in the lowest energy state ($n_x = n_y = n_z = 0$). It is given by $\phi(\mathbf{r_1}, ..., \mathbf{r}_N) = \prod_i \varphi_0(\mathbf{r_i})$ where

$$\varphi_0(\mathbf{r_i}) = \left(\frac{m\omega_{\rm ho}}{\pi\hbar}\right)^{3/2} \exp\Big[- \frac{m}{2\hbar}(\omega_x^2 x^2 + \omega_y^2 y^2 + \omega_z^2 z^2)\Big] \tag{10}$$

and $\omega_{\rm ho} = (\omega_x\omega_y\omega_z)^{1/3}$.The density distribution of this system becomes $n(\mathbf{r}) = N|\varphi_0(\mathbf{r})|^2$. Eq.(10) has a Gaussian density profile with an average width of $a_{\rm ho}$ defined as

$$a_{\rm ho} = \left(\frac{\hbar}{m\omega_{\rm ho}}\right)^{\frac{1}{2}}. \tag{11}$$

A plot of the condensate and thermal density of 5000 non−interacting particles in a harmonic trap at temperature $T = 0.9T_c^0$ is included in Fig.2, where T_c^0 is the temperature at which condensation occurs. The Fourier transformation of the ground state wave-function enables one to calculate the momentum distribution of the atoms within the condensate. It can be seen that the momentum distributions of the condensed and non-condensed particles of an ideal gas have the exact same form as the density distributions n_0 and n_T respectively.

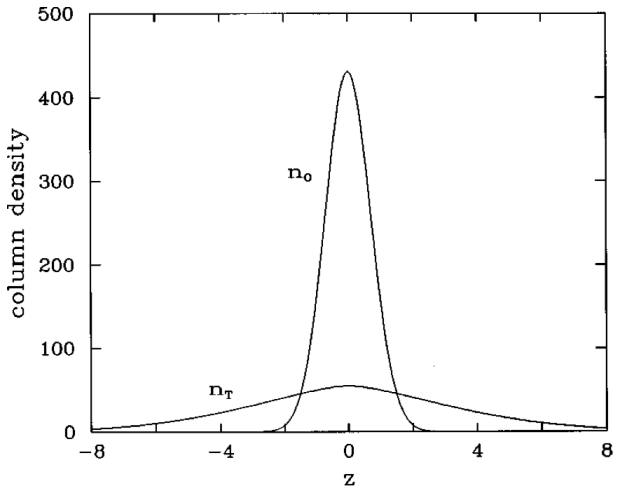

Figure 2: Column density for 5000 non-interacting bosons in a harmonic trap at $T = 0.9T_c^0$. The tall and broader central peaks are of the condensate and the thermal distribution respectively. The distance and density are in units of $a_{\rm ho}$ and $a_{\rm ho}^{-2}$ respectively with the density normalized to the number of atoms. The same curves can be identified with momentum distribution if the coordinate and momentum distribution are in units of $a_{\rm ho}^{-1}$ and $a_{\rm ho}^2$ respectively. Figure reproduced from Ref. [9]

If interactions are included in this system of harmonically trapped bosons ($g \neq 0$ in Eq.(7)) then the shape of the condensate can change significantly from a Gaussian when no interactions are considered. The scattering

length, a, defined in Eq.(75) can be either positive or negative with its sign and magnitude depending on the atom-atom potential. The interaction also has a large effect on the dynamics and thermodynamics of the system.

The ground state can be obtained using mean-field theory as the wave-function of the condensate can be written as $\Psi(\mathbf{r},t) = \Phi(\mathbf{r})\exp(-i\mu t/\hbar)$ where μ is the chemical potential and ϕ is real. With ϕ normalized to the total number of particles by $\int d\mathbf{r}\phi^2 = N_0 = N$. The GPE becomes

$$\Big(-\frac{\hbar^2}{2m}\nabla^2 + V_{\text{ext}}(\mathbf{r}) + g\phi^2(\mathbf{r})\Big)\phi(\mathbf{r}) = \mu\phi(\mathbf{r}), \tag{12}$$

which has the form of a "non-linear Schrödinger equation". The non-linearity comes from the mean field term being proportional to the particle density given as $n(\mathbf{r}) = \phi^2(\mathbf{r})$. Numerical solutions of the GPE in the form of Eq.(12) are relatively easy to obtain and are the subject of Ref. [11–15].

C. Deriving The Equations Of Motion For Bose-Einstein Condensates In A Double Well

The rest of this section will discus the non-interacting Bose gas in a symmetric double well as seen in Fig.3. In this model, the phase coherence is an important property of BECs. An interesting manifestation of phase coherence in trapped condensates are the possibilities of Josephson-type effects. These are analogous to the well known properties of Josephson junctions that occur in superconductors and super-fluids mentioned in Sec.IB.. If the barrier between the two wells is high enough then the GPE has two natural solutions defined as $\phi_1(\mathbf{r})$ and $\phi_2(\mathbf{r})$ which are localized in each potential well with a chemical potential μ_1 and μ_2 respectively. The chemical potential of the two traps can vary by filling each trap with a different number of atoms. The overlap between the two condensates only occurs in the classically forbidden region. This type of system is what is considered to be a weakly linked BEC.

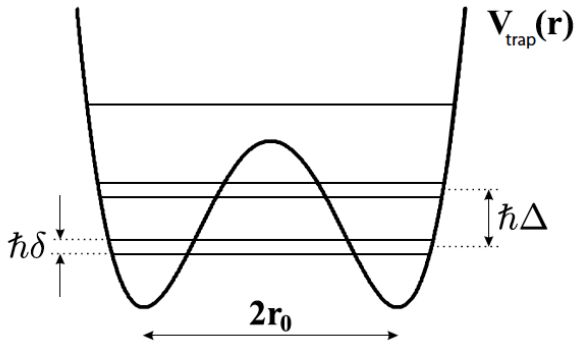

Figure 3: Schematic representation of the double well level structure. Levels below the potential barrier are almost two fold degenerate with their energy differences characterizing the tunnel coupling. Typically, the inter-level spacing between levels $1\hbar\delta$ and $2\hbar\delta$ is much smaller than the spacing between $2\hbar\delta$ and $3\hbar\delta$. Figure reproduced from Ref. [16].

D. Analytic Solution Of The Equations Of Motion

If the potential barrier is high, the two wells are completely isolated and their single particle eigenstates of energy $\hbar\Delta$ are those of an an-harmonic oscillator of trap frequency ω_0 such that $\hbar\Delta = \hbar\omega_0$. For a low potential barrier, the two lowest symmetric and anti-symmetric states of the system are delocalised over both wells with their energy difference $\hbar\delta$ describes the tunnel coupling [16]. The system under consideration will be where $\Delta \gg \delta$ where only the symmetric and anti-symmetric state are needed to describe the system. This system is what is typically known as the double-well Bose-Einstein condensate which is generally a good approximation when the symmetric and anti-symmetric states are separated from higher modes. However, it is not such a good approximation when there are strong atom-atom interactions or when there is a very low potential barrier. A generic double well potential can be defined as

$$V_{\text{trap}}(\mathbf{r}) = \frac{m\omega_0}{8r_0^2}(r^2 - r_0^2)^2, \tag{13}$$

where $\pm r_0$ is the position of the potential minima, ω_0, is the single well oscillation frequency and $m\omega_0^2 r_0^2/8$ is the barrier height. This can approximate the well in Fig.3 to within a few percent. The on-well oscillation frequency ω_0 is fixed so only varying the trap separation r_0 modifies the tunnel coupling. The Hamiltonian of the non interacting system is $H_0 = p^2/(2m) + V_{\rm trap}(r)$. The ground state $|\Phi_{\rm sym.}\rangle$ of the double well given by Eq.(13) is delocalized over both well and is symmetric. $|\Phi_{\rm antsym.}\rangle$ is equally delocalized but anti-symmetric [17]. The completely localized states $|\phi_1\rangle$ and $|\phi_2\rangle$ are given by

$$\begin{aligned} |\phi_1\rangle &= \frac{1}{\sqrt{2}}(|\Phi_{\rm sym.}\rangle + |\Phi_{\rm antsym.}\rangle), \\ |\phi_2\rangle &= \frac{1}{\sqrt{2}}(|\Phi_{\rm sym.}\rangle - |\Phi_{\rm antsym.}\rangle), \end{aligned} \tag{14}$$

respectively. It is important to note that these are not proper eigenstates of the Hamiltonian. This is because the system prepared in the localized state $|\phi_1\rangle$ will evolve to $|\phi_2\rangle$ and back with frequency δ which is defined by the energy difference $\hbar\delta$ between the eigenstates $|\Phi_{\rm sym.}\rangle$ and $|\Phi_{\rm antsym.}\rangle$.

E. The Bose Josephson Junction

In the limit that the particle interaction energy is small in comparison to the single particle energy, the particles occupying the two lowest eigenstates of the Hamiltonian are considered. The non-linear interaction term is neglected in this region giving a time dependent variational wave-function defined as:

$$\Psi(\mathbf{r}, t) = \psi_1(t)\phi_1(\mathbf{r}) + \psi_2(t)\phi_2(\mathbf{r}), \tag{15}$$

where $\phi_1(\mathbf{r})$ and $\phi_2(\mathbf{r})$ are the localized states defined by Eq.(14). The terms $\psi_1(t)$ and $\psi_2(t)$ are defined by:

$$\begin{aligned} \psi_1(t) &= \sqrt{N_1}e^{i\theta_1(t)}, \\ \psi_2(t) &= \sqrt{N_2}e^{i\theta_2(t)}, \end{aligned} \tag{16}$$

where $N_1 + N_2 = |\psi_1|^2 + |\psi_2|^2 = N$, and θ_1, θ_2 are the phases in the trap left and right respectively. N is the total number of atoms. By substituting the wave-function given in Eq.(15) in to the GPE, the following set of coupled differential equations are obtained:

$$i\hbar\frac{\partial}{\partial t}\psi_1 = (E_1 + U_1 N_1)\psi_1 - K\psi_2, \tag{17}$$

$$i\hbar\frac{\partial}{\partial t}\psi_2 = (E_2 + U_2 N_2)\psi_2 - K\psi_1, \tag{18}$$

where K is the coupling constant [18]. Damping and finite temperature effects are ignored. A more complete derivation of Eq.(17-18) including the neglected terms is included in Sec.IIK.. E_1 and E_2 are defined as the energy of the localized left and right state in with the absence of interactions and are defined as:

$$\begin{aligned} E_1 &= \int \left[\frac{\hbar^2}{2m}|\nabla\phi_1|^2 + |\phi_1|^2 V\right] dr, \\ E_2 &= \int \left[\frac{\hbar^2}{2m}|\nabla\phi_2|^2 + |\phi_2|^2 V\right] dr, \end{aligned} \tag{19}$$

respectively. The nonlinear interaction energy is described by the terms $U_1 N_1$ and $U_2 N_2$ respectively, where U_1 and U_2 are defined as

$$\begin{aligned} U_1 &= g\int |\phi_1|^4 dr, \\ U_2 &= g\int |\phi_2|^4 dr. \end{aligned} \tag{20}$$

The coupling energy K is defined as

$$K = -\int \left[\frac{\hbar^2}{2m}(\nabla\phi_1\nabla\phi_2) + \phi_1 V\phi_2\right] dr. \tag{21}$$

It is useful to define the phase difference $\phi(t)$ as

$$\phi(t) = \theta_2 - \theta_1, \qquad \phi(t) \in [0, 2\pi], \tag{22}$$

and the atom number population difference $z(t)$ as

$$z(t) = \frac{N_1(t) - N_2(t)}{N} \equiv \frac{|\phi_1|^2 - |\phi_2|^2}{N}, \qquad z(t) \in [-1, 1]. \tag{23}$$

Eq.(17-18) are solved in Appendix.B to give:

$$\dot{z}(t) = -\sqrt{1 - z^2(t)} \sin \phi(t) \tag{24}$$

and

$$\dot{\phi}(t) = \Delta E + \Lambda z(t) + \frac{z(t)}{\sqrt{1 - z^2(t)}} \cos \phi(t). \tag{25}$$

These two equations are useful as they completely describe the dynamics of the coupled system. The chemical potential difference is also described by $\Delta\mu = \hbar\dot{\phi}$. The dimensionless parameters, ΔE and Λ are defined as

$$\Delta E = \frac{(E_1 - E_2)}{2K} + \frac{(U_1 - U_2)N}{4K} \tag{26}$$

and

$$\Lambda = \frac{(U_1 + U_2)N}{4K}. \tag{27}$$

The Hamiltonian of this system derived in terms of the new variables is

$$H = \frac{\Lambda z^2}{2} + \Delta E z - \sqrt{1 - z^2} \cos \phi, \tag{28}$$

where the coordinates $z(t)$ and $\phi(t)$ are canonically conjugate with

$$\dot{z} = \frac{\partial H}{\partial \phi} \qquad \text{and} \qquad \dot{\phi} = \frac{\partial H}{\partial z}. \tag{29}$$

In a simple mechanical analogy, H can be thought of as describing a non-rigid pendulum of tilt angle ϕ and length proportional to $\sqrt{1 - z^2}$ that decreases with the angular momentum z [19].

III The Double Well Bose-Einstein Condensate

The Symmetric Trap occurs when $\Delta E = 0$ in the coupled equations Eq.(31) and Eq.(30). Thus, the equations of motion read as

$$\dot{z}(t) = -\sqrt{1 - z^2(t)} \sin \phi(t) \tag{30}$$

and

$$\dot{\phi}(t) = \Lambda z(t) + \frac{z(t)}{\sqrt{1 - z^2(t)}} \cos \phi(t). \tag{31}$$

In this section, Eq.(30-31) will be solved for various parameters using a Runge-Kutta method. The behaviour of the systems will then be discussed.

A. Non-Interacting limit

For non-interacting atoms, when $\Lambda = 0$, Eq.(30-31) describe sinusoidal Rabi-like oscillations in the population of each trap with a frequency $\omega = 2K$ in dimensionless units. These types of oscillations are equivalent to describing a single atom rather than the Josephson effect that otherwise arrises from an interacting super-fluid condensate.

B. Small-Amplitude Oscillations

In the limit where $|z| \ll 1$ and $|\phi| \ll 1$, Eq.(30-31) become linear and simplify to:

$$\dot{z} \simeq -\phi, \tag{32}$$

$$\dot{\phi} \simeq (\Lambda + 1)z. \tag{33}$$

Using the non-rigid pendulum analogy, the equations describe small amplitude oscillations of a pendulum with a sinusoidal function, $z(t)$, with a frequency given as

$$\omega_L = \sqrt{2UNK + 4K^2} \tag{34}$$

in dimensionless units. The frequency, ω_L, is independent of the initial conditions $z(0)$ and $\phi(0)$.

C. Solving the Equations of Motion of the Symmetric Trap in the non-linear regime

Eq.(30-31) can also be solved numerically for a non-zero dimensionless parameter Λ. The solutions are sinusoidal oscillations that are the an-harmonic generalization of the Josephson effects [19]. By keeping the initial conditions the same, one can plot z as a function of t for different values of Λ. Eq.(30-31) were solved numerically with the use of a Runge-Kutta method. The results are produced with the initial conditions $z(0) = 0.6$ and $\phi(0) = 0$ for $\lambda = 1$, 8, 9.99, 10, 11 in Fig.4. For $\lambda = 1$, 8, an oscillation can be seen indicating that the particles tunnel back and forth between the two wells as time increases.

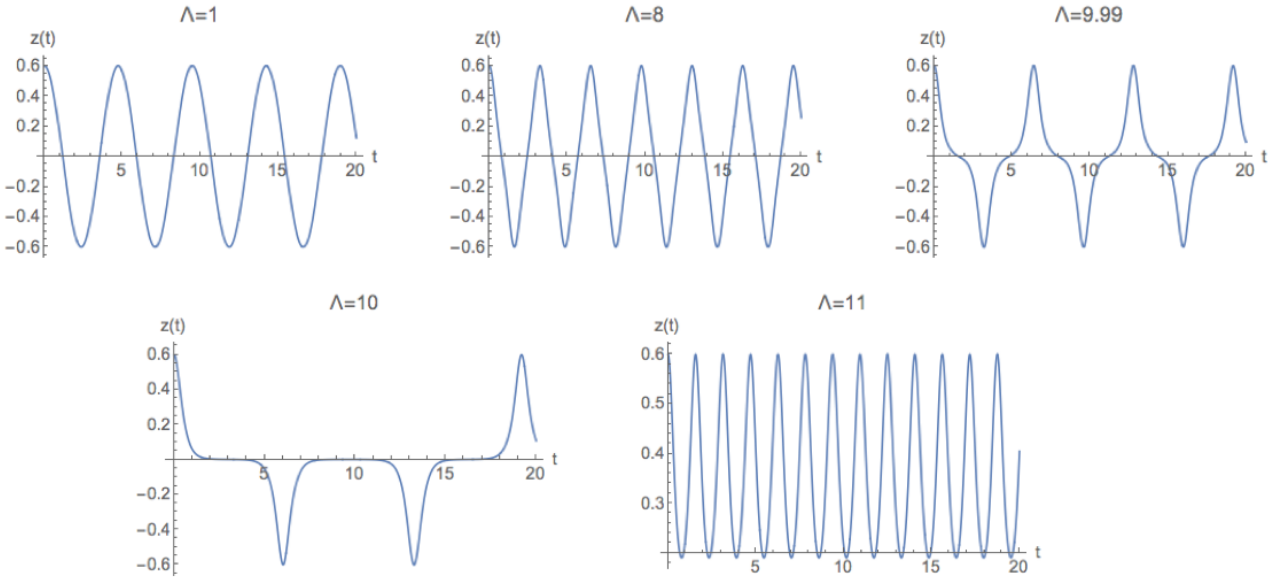

Figure 4: Numeric solution of Eq.(30-31) with initial conditions $z(0) = 0.6$ and $\phi(0) = 0$ for different values of Λ. $z(t)$ is plotted against t for Λ =1,8,9.99,10 and 11 for which a critical transition occurs at $\Lambda = 10$.

A better understanding of Fig.4 is possible by looking at the phase difference, $\phi(t)$ as well as $z(t)$. For the initial conditions ($z(0) = 0.5$ and $\phi(0) = 0$), ϕ and z are plotted as a function of t for $\lambda = 1$, 8, 9.99, 10, 11 in Fig.5. The non-rigid pendulum mentioned in Sec.IIE. is a useful analogy that can be used to explain the system. In Fig.5, for $\Lambda = 1$ and $\Lambda = 5$, an expected sinusoidal oscillation occurs where T_z and T_ϕ, the period of $z(t)$ and $\phi(t)$ become the same. This is because

$$\lim_{\Lambda \to 0} T_z = T_\phi \tag{35}$$

as the system is close to the non-interacting limit. This is also the regime which describes Rabi-like oscillations previously discussed in Sec.IIIA..

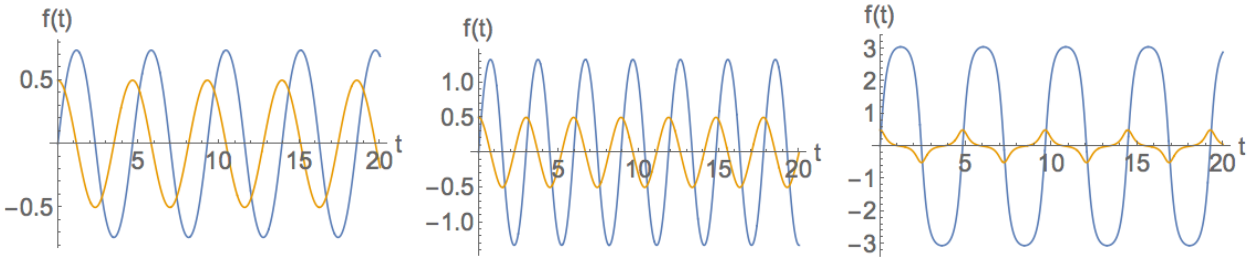

(a) (b) (c)

Figure 5: The atom number population difference, $z(t)$ in orange, and phase difference, $\phi(t)$ in blue as a function of time plotted for $\lambda = 1$, 5, 14.9 in Pane.(a), Pane.(b) and Pane.(c) respectively. The initial conditions were set to $z(0) = 0.5$ and $\phi(0) = 0$.

The sinusoidal oscillations become an-harmonic when Λ is increased. There is a crossover transition for $\Lambda = \Lambda_C = 10$ where the oscillation is no longer sinusoidal. For large Λ, the population in each well oscillates around a non zero-point in contrast to the case with small Λ. This is because as Λ increases, there is a diversion from the non-interacting case. This is due to Λ acting as a coupling constant and so as Λ increases, the interactions become stronger. For $\Lambda = \Lambda_C = 10$, the oscillations not only oscillate around a non-zero point but they also become an-harmonic. This is also better understood using the non-rigid pendulum analogy. In this regime, the angular momentum, $z(0)$, is sufficiently large to swing the pendulum over the vertical orientation corresponding to $\phi = \pi$. This is possible as the non-zero average angular momentum, $z(t)$ corresponds to the rotatory motion depends on the initial condition of Λ_C. From the Hamiltonian, Eq.(28), the value $z(t) = 0$ is inaccessible at any time if $\Lambda > \Lambda_c$ where

$$\Lambda_c = 2\left(\frac{\sqrt{1 - z(0)^2}\cos\phi(0) + 1}{z(0)^2}\right). \tag{36}$$

The oscillations about a non-zero point arise because of the inter-atomic interactions within the Bose gas. The interactions are quantum mechanical in nature and are due to a a phenomenon known as macroscopic quantum self trapping (MQST) [19]. In Fig.5, when $\Lambda = 14.9$, the particle in-balance, $z(t)$, becomes increasingly out of sync with the phase difference $\phi(t)$. This regime is known as the running phase model. Using the pendulum analogy and thinking of $\phi(t)$ as the angular displacement of the pendulum, $\Lambda = 14.9$ in Fig.5 describes a pendulum with sufficient energy to complete a full rotation.

D. Changing the initial conditions of the system

A regime of an-harmonic oscillations can be observed by plotting $z = (N_1 - N_2)/N_T$ as a function of time. This can be seen in Fig.6 where $\Lambda = 10$ and $\phi(0) = 0$ and $z(0)$ takes the values 0.1, 0.5, 0.59, 0.6 and 0.65 in Fig.6(a-e) respectively. Increasing Λ for fixed $z(0)$ as the case in Fig.4 or increasing $z(0)$ for fixed Λ is what adds higher harmonics to the sinusoidal oscillations. This corresponds to large amplitude oscillations of the non-rigid pendulum which can be seen in Fig.6(b) and Fig.6(c). The period of these oscillations increase as $z(0)$ increases and then decrease, undergoing a critical slowdown when $z(0) = 0.6$ as seen in Fig.6(d) when logarithmic divergence occurs. The singularity in Fig.6(d) represent the pendulum in a vertically upright position.

E. π-Phase Modes

The crossover parameter for MQST occurs when the in-equality in Eq.(36) becomes an equality. If $\phi(0)$ and Λ are kept constant with $z(0)$ being changes as the case in Fig.6, then a critical population balance, z_c, can be defined. z_c can be defined such that when $z(0)$ and $\phi(0)$ are substituted into the Hamiltonian becomes

$$H_0 \equiv H(z(0), \phi(0)) = \frac{\Lambda}{2}z(0)^2 - \sqrt{1 - z(0)^2}\cos[\phi(0)] > 1. \tag{37}$$

For $\phi(0) = 0$, as the case in Fig.4 and Fig.6, MQST occurs when $z(0) > z_c$. However for the case when $\phi(0) = \pi$, MQST occurs when $z_c > z(0)$ as the case in Fig.7. These π-phase modes describe the tunneling dynamics when the time averaged value of the phase across the junction is equal to π, i.e. $\langle\phi(t)\rangle = \pi$.

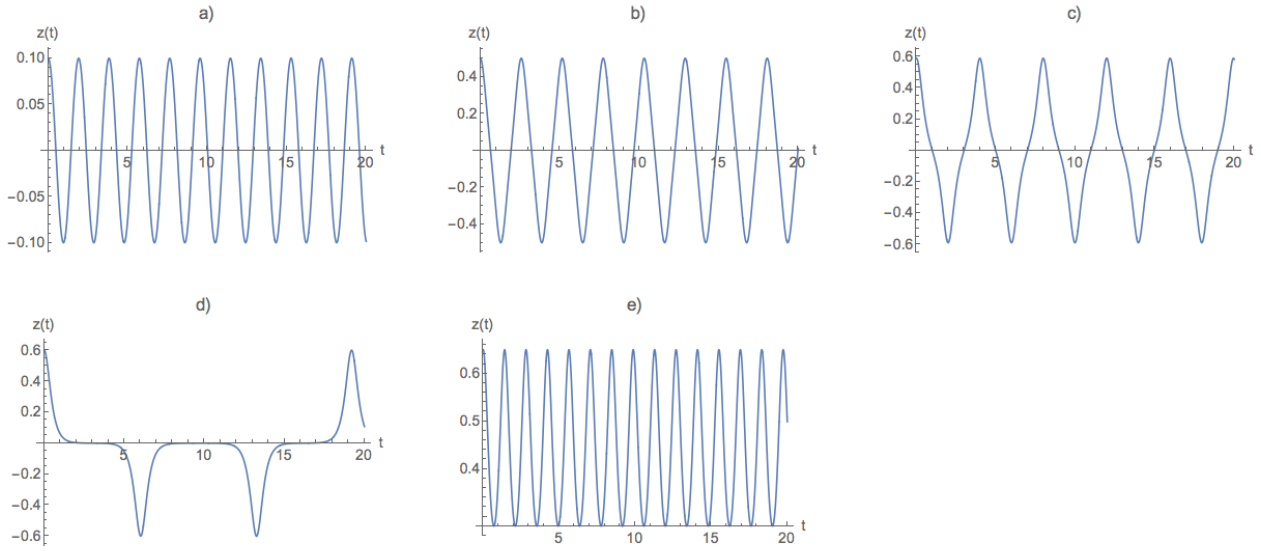

Figure 6: Population imbalance, $z(t)$, as a function of dimensionless time with $\Lambda = 10$ and $\phi(0) = 0$. The initial conditions for $z(0)$ takes the values a) 0.1, b) 0.5, c) 0.59, d) 0.6 and e) 0.65 respectively.

For $H_0 > 1$, $\langle z(t)\rangle \neq 0$ with oscillations about the non-zero value. If $H_0 < 1$, $\langle z(t)\rangle = 0$. MQST arises from the self interaction of the atoms. This self interaction is dependent on the initial conditions, the total number of atoms and the trap parameters.

Using the pendulum analogy, if the initial angular kinetic energy of the pendulum, $z^2(0)$, exceeds the potential energy barrier of vertical displacement $\phi = \pi$, a pendulum rotation will occur with non zero angular momentum. This is a closed-loop trajectory around the pendulum.

F. Small-Amplitude Oscillations around a fixed point

For small z, Eq.(24-25) can be linearised around a fixed point defined as $Z_s = 0$ giving harmonic oscillations for $\lambda < 1$ [18]. Eq.(24) can be linearied in z giving a Bose Josephson Junction (BJJ) equation of the form

$$\ddot{\phi} = -\big(\Lambda \sin(\phi) + \frac{1}{2}\sin(2\phi)\big) + \mathcal{O}(z^2). \tag{38}$$

Using the pendulum analogy, suggests that there is a particle of spacial coordinate ϕ that moves in the potential

$$V(\phi) = -\Lambda\cos(\phi) - \frac{1}{4}\cos(2\phi) + \mathcal{O}(\phi^2). \tag{39}$$

For large-amplitude oscillations, the momentum dependent length of the pendulum's allows the pendulum's bob to make oscillations with $\langle z(t)\rangle = 0$ around the vertical axis. Λ can also exceed unity for large amplitudes of $z(t)$ as the case in Fig.7(b).

G. Oscillations With Macroscopic Quantum Self-Trapping

The pendulum can also make a closed $\langle z(t)\rangle \neq 0$ rotation around the top of the vertical. MQST occurs for two different types of π-phase modes. The first occurs when the time average, $\langle z\rangle < |z_s| \neq 0$, where z_s is the z-symmetric breaking value of the GPE. These two types of MQST can be seen in Fig.7(d) and Fig.7(f) respectively. In Fig.7(d), there is a changeover between the two states that is represented by the straight line in Fig.7(e). Once Λ exceeds the value $\Lambda_s = 1/\sqrt{1 - z(0)^2}$, the system transitions to the second trap state seen in Fig.7(f).

H. Phase Plots

A phase portrait of the two dynamical variables z and ϕ can be used to better understand the dynamical behaviour of the BJJ system. This is done in Fig.8 where the trajectories calculated for different values of Λ for the initial conditions $z(0) = 0.6$.

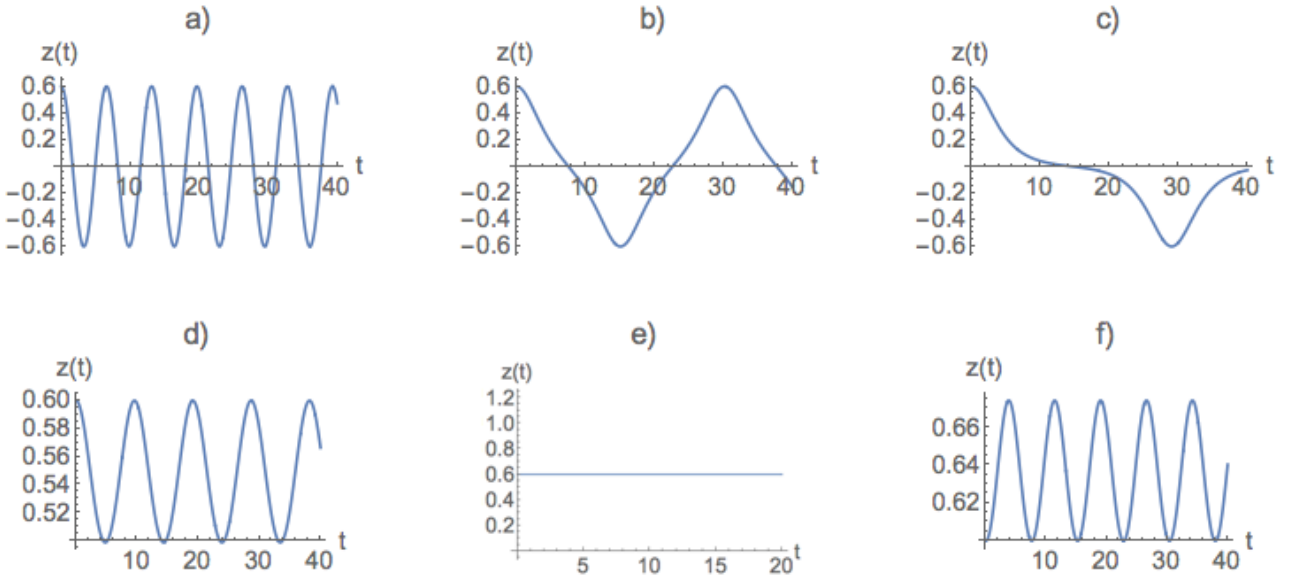

Figure 7: Population imbalance, $z(t)$, as a function of dimensionless time with $z(0) = 0.6$ and $\phi(0) = \pi$. The initial conditions for Λ takes the values a) 0.1, b) 1.1, c) 1.111, d) 1.2, e) 1.25 and f) 1.3 respectively.

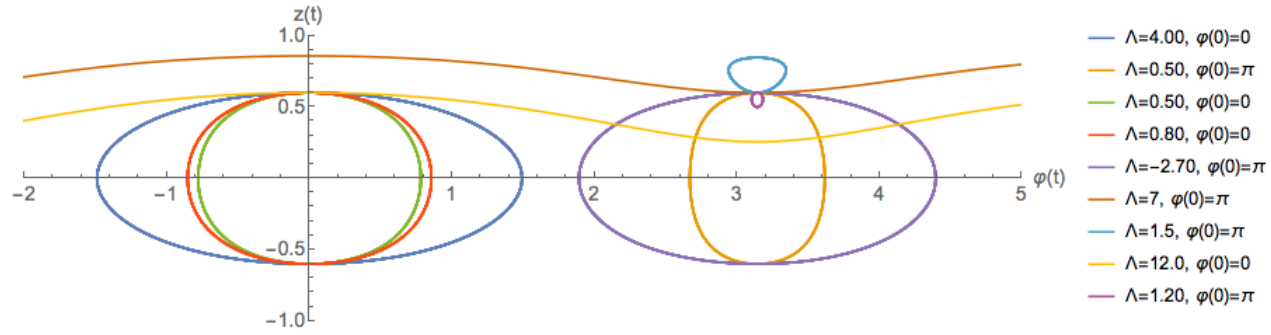

Figure 8: Phase portraits for $z(0) = 0.6$ for $\phi(0) = \pi$, $\phi(0) = 0$ and various values for Λ.

In Fig.8, the running mode MQST can be seen for $\Lambda = -12.0$ and $\phi(0) = 0$. Where $\phi(0) = 0$ and $\Lambda = 4$, $\Lambda = 0.5$, $\Lambda = 0.8$ describe when the evolution for when the phase, ϕ oscillated around 0 and $\langle z(t)\rangle = 0$. For a rigid pendulum, without the $\sqrt{1 = z^2}$ term in the Hamiltonian given in Eq.(28), only the curves described thus far can be obtained. However, due to the momentum dependence in the potential in the Hamiltonian, Eq.(28) for the BJJ there is much more richness in the solutions. All of which correspond to $\phi(0) = \pi$. An important thing to notice is that as Λ/Λ_c defined in Eq.(36) increases and approaches 1, the area enclosed by the trajectories and is pinched at $\Lambda = \Lambda_c$. This marks the onset of π-phase MQST where $\langle z(t)\rangle < |z_s|$ where z_s is the stationary z-symmetry breaking state as seen in the trajectory where $\Lambda = 1.20$ and $\phi(0) = \pi$. Further increasing Λ/Λ_c results in a reflection of the trajectory of the fixed point at which π-phase $\langle z(t)\rangle > |z_s|$ MQST occurs as seen when $\Lambda = 1.00$ and $\phi(0) = \pi$.

I. The Asymmetric Double Well

The trap becomes asymmetric when $\Delta E \neq 0$ is set such that the Hamiltonian reads

$$H = \frac{\Lambda z^2}{2} + \Delta E z - \sqrt{1 - z^2}\cos\phi. \tag{40}$$

Thus the equations of motion are Eq.(24-25) which are re-written here for convenience as

$$\dot{z}(t) = -\sqrt{1 - z^2(t)}\sin\phi(t) \tag{41}$$

and

$$\dot{\phi}(t) = \Delta E + \Lambda z(t) + \frac{z(t)}{\sqrt{1 - z^2(t)}} \cos\phi(t). \tag{42}$$

There is an interesting regime that occurs when the energy gap, ΔE, between the well is large. Mathematically, this occurs when $\Lambda z(0) \ll \Delta E$ as the non rigid pendulum is driven to rotate in a direction that is determined by ΔE which corresponds to a Josephson-like effect.

In Sec.IIIC., with $\Delta E = 0$ and $\Lambda > \Lambda_{\mathbf{c}}$, defined in Eq.(36), it was stated that the pendulum experiences oscillatory motion in a direction that depends on $z(0)$. For the case that $\Lambda z(0) \gg \Delta E$, it is also that this motion persists. This motion corresponds to MQST which is due to non-linearity.

J. The Asymmetric Trap Plots

The effects of setting $\Delta E \neq 0$ can be seen in Fig.9 for the initial conditions $z(0) = 0.5$, $\Lambda = 1$, $\phi(0) = \pi/2$ for three different values of ΔE.

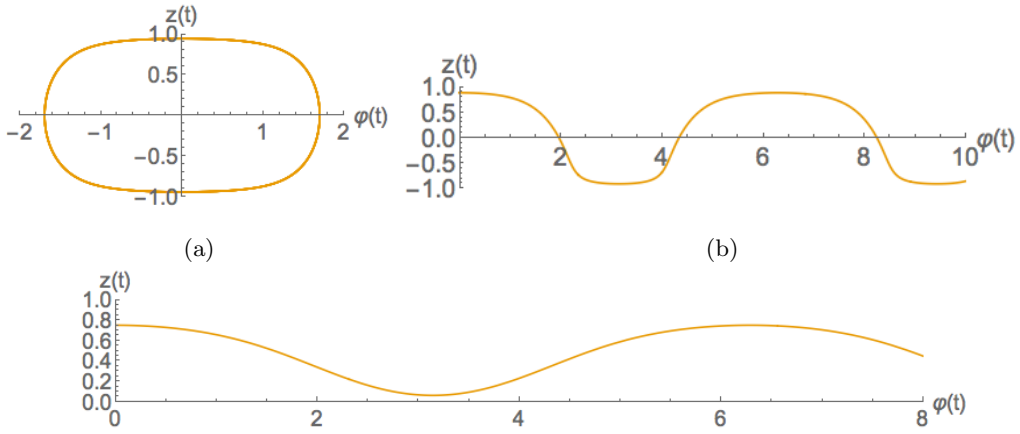

Figure 9: $z(t)$ and $\phi(t)$ plotted as a function of t for the initial conditions $z(0) = 0.6$, $\Lambda = 1$, $\phi(0) = \pi/2$ and $\Delta E = 0, 0.5, 2$ in Pane.a, Pane.b and Pane.c respectively.

Fig.9(a) shows the symmetric trap case in the zero-phase mode which has previously been discussed. Fig.9(b) shows self trapping occurring in a running phase. This is looked at in more detail in Fig.10 where $z(t)$ and $\phi(t)$ is plotted as a function of t. Fig.9(c) shows a new regime that only occurs when there is a relatively large energy gap. If the energy gap was symmetric the only zero or π-phase oscillations would be observed.

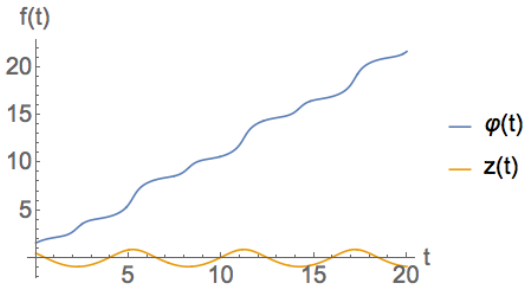

Figure 10: $z(t)$ and $\phi(t)$ plotted as a function of t for the initial conditions $z(0) = 0.5$, $\Lambda = 1$, $\phi(0) = \pi/2$ and $\Delta E = 0.5$.

Fig.10 is of particular interest as self trapping occurs however, there is also a running phase. Another interesting property is that the amplitude of the Josephson oscillation is greater than the initial particle inbalance. Using the mechanical analogy, this is equivalent to the pendulum rotating about the pivot continually

where the time average of the length is constant. $\langle z(t)\rangle$, the time averaged particle in-balances is not equal to zero as the oscillation is an-harmonic. The particle in-balance could be in favour of either well.

Fig.11 shows further results for the energy difference, $\Delta E = 0.5$ for various parameters.

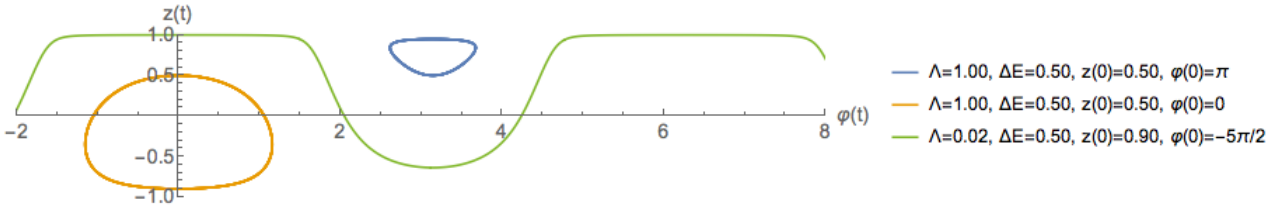

Figure 11: Phase portraits for various values of $z(0), \phi(0), \Lambda$ and ΔE.

K. Including the neglected terms in the GPE

Eq.(17-18) can be re-derived to include the previously neglected terms. This is done in Appendix.C giving the result:

$$i\hbar\frac{\partial\psi_1}{\partial t} = (E_1 + U_1N_1)\psi_1 + K\psi_2 + g_0\Big(\psi_2(t)^3\int d2\phi_1^*(\mathbf{r})\phi_2(\mathbf{r})^3 + 3\psi_1(t)\psi_2^2(t)\int d2|\phi_1(\mathbf{r})|^2\phi_2(\mathbf{r})^2 + 3\psi_1(t)^2\psi_2(t)\int d2|\phi_1(\mathbf{r})|^3\phi_2(\mathbf{r})\Big). \tag{43}$$

This equations can be further simplified by naming the previously neglected terms $U_{\alpha,\beta,\gamma,\delta}$ where $\alpha, \beta, \gamma, \delta$ represent the spacial part of wave-function within the integral. This gives the definitions:

$$U_{1111} = g_0\int d\mathbf{r}|\phi_1(\mathbf{r})|^4, \tag{44}$$

$$U_{1112} = g_0\int d\mathbf{r}|\phi_1(\mathbf{r})|^3\phi_2(\mathbf{r}), \tag{45}$$

$$U_{1122} = g_0\int d\mathbf{r}|\phi_1(\mathbf{r})|^2|\phi_2(\mathbf{r})|^2, \tag{46}$$

$$U_{1222} = g_0\int d\mathbf{r}\phi_1^*(\mathbf{r})|\phi_2(\mathbf{r})|^3. \tag{47}$$

Using these definitions, Eq.(43) can be written in a more compact form as:

$$i\hbar\frac{\partial\psi_1}{\partial t} = (E_1 + U_{1111}N_1)\psi_1 + K\psi_2 + U_{1222}\psi_2(t)^3 + 3U_{1122}\psi_1(t)\psi_2(t)^2 + 3U_{1112}\psi_1(t)^2\psi_2(t). \tag{48}$$

L. Accounting For The U_{1122} Term

Taking into account the U_{1122} term in Eq.(48), the coupled differential equations Eq.(17-18) are modified to

$$i\hbar\frac{\partial}{\partial t}\psi_1 = (E_1 + U_{1111}N_1)\psi_1 + K\psi_2 + 3U_{1122}\psi_1(t)\psi_2(t)^2, \tag{49}$$

$$i\hbar\frac{\partial}{\partial t}\psi_2 = (E_2 + U_{2222}N_2)\psi_2 + K\psi_1 + 3U_{2211}\psi_1(t)^2\psi_2(t). \tag{50}$$

These equations are solved in Appendix.D giving the results

$$\dot{z}(t) = \sqrt{1-z^2}\sin\phi - 6U_{1122}N_1N_2\cos(2\theta_1 - \phi)\sin\phi \tag{51}$$

$$\dot{\phi}(t) = (N_1U_{1111} - N_2U_{2222}) - \frac{z}{\sqrt{1-z^2}}\cos\phi + 12U_{1122}N_1N_2\cos\left(\frac{2\theta_1-\phi}{2}\right)\sin\phi. \tag{52}$$

Whats important to note from these equations is that they are similar to the case where the U_{1122} term is neglected as defined in Eq.(24-25). However, the extra terms mean that the symmetric well behaves an-harmonically as a result of the extra $\cos(2\theta_1 - \phi)$ terms.

IV The Triple Well Bose-Einstein Condensate

A triple well system is now considered. A cartoon of this setup is included in Fig.12. Three phase difference and population differences describing the triple well can be derived in a similar case as to the double well which was described in Appendix.C. Instead of the ansatz defined in Eq.92, the ansatz

$$\Psi(\mathbf{r},t) = \psi_1(t)\phi_1(\mathbf{r}) + \psi_2(t)\phi_2(\mathbf{r}) + \psi_3(t)\phi_3(\mathbf{r}) \tag{53}$$

is substituted into Eq.(76) (the GPE). The derivation giving the six equations of motion, Eq.(124-129), is highlighted in Appendix.E. A useful relation is defined as

$$\phi_{21} + \phi_{32} = \phi_{31}. \tag{54}$$

This means that Eq.(125) and Eq.(126) are only needed to completely describe ϕ as opposed to three. A useful sanity check is to realize that in the case of the triple well, the total number of particles defined as $N_{\text{tot}} = N_3 + N_2 + N_1$ is conserved. Because of this, N_{tot} is a constant and so

$$\dot{N}_1 + \dot{N}_2 + \dot{N}_3 = 0 \tag{55}$$

can be used to verify that the equations of motion calculated are correct. For this reason, Eq.(127) and Eq.(129) which describe the particle imbalances z_{21} and z_{32} respectively will be considered. This reduces the amount of simultaneous equations down to four and are:

$$\dot{\phi}_{21}(t) = (E_2 - E_1) + (U_2N_2 - U_1N_1) + K_{12}\left(\sqrt{\frac{N_1}{N_2}} - \sqrt{\frac{N_2}{N_1}}\right)\cos\phi_{21} - K_{13}\sqrt{\frac{N_3}{N_1}}\cos\phi_{31} + K_{32}\sqrt{\frac{N_3}{N_2}}\cos\phi_{32}, \tag{56}$$

$$\dot{\phi}_{32}(t) = (E_3 - E_2) + (U_3N_3 - U_2N_2) + K_{32}\left(\sqrt{\frac{N_2}{N_3}} - \sqrt{\frac{N_3}{N_2}}\right)\cos\phi_{32} - K_{21}\sqrt{\frac{N_1}{N_2}}\cos\phi_{21} + K_{31}\sqrt{\frac{N_1}{N_3}}\cos\phi_{31}, \tag{57}$$

$$\dot{z}_{21}(t) = \frac{4K_{12}\sqrt{N_1N_2}\sin\phi_{21} - 2K_{23}\sqrt{N_2N_3}\sin\phi_{32} + 2K_{13}\sqrt{N_1N_3}\sin\phi_{31}}{N_1 + N_2 + N_3}, \tag{58}$$

$$\dot{z}_{32}(t) = \frac{4K_{32}\sqrt{N_3N_2}\sin\phi_{32} - 2K_{13}\sqrt{N_1N_3}\sin\phi_{31} + 2K_{12}\sqrt{N_1N_2}\sin\phi_{21}}{N_1 + N_2 + N_3}. \tag{59}$$

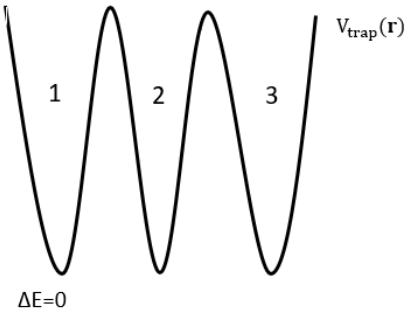

Figure 12: A cartoon of the triple well setup.

A. The simplest case for the Triple Well Bose-Einstein Condensate

The simplest case for the equations occurs when the triple well trap is symmetric such that $E_1 = E_2 = E_3 = 0$ and $U_1 = U_2 = U_3 = 1$. A realistic number of particles, N_{tot}, is of the order $10,000$ is considered. Thus, the particle imbalance will be set as $N_1 = N_2 = N_3 = 3000$ such that $N_{\text{tot}} = 9000$. K can be estimated using Eq.(27) and in this simulation, the coupling energies will be set as $K_{12} = K_{31} = K_{32} = K = 5000$. Using these values for the parameters, the four equations of motion are rather simple and given as:

$$\frac{\dot{\phi}_{21}}{5000} = \cos\phi_{32} + \cos(\phi_{21} + \phi_{32}), \tag{60}$$

$$\frac{\dot{\phi}_{32}}{5000} = -\cos\phi_{21} + \cos\left(\phi_{21} + \phi_{32}\right), \tag{61}$$

$$\frac{3\dot{z}_{21}}{10000} = 2\sin\left(\phi_{21}\right) - \sin\phi_{32} + \sin\left(\phi_{21} + \phi_{32}\right), \tag{62}$$

$$\frac{3\dot{z}_{32}}{10000} = 2\sin\phi_{32} + \sin\left(\phi_{21} + \phi_{32}\right) - \sin\phi_{21}. \tag{63}$$

These are solved simultaneously using a Runge-Kutta method. As expected, there are no oscillations observed between the three wells for the zero-phase mode. This also indicates that the code created is working correctly. An example of the code used to solve both $\phi(t)$ and $z(t)$ is included in Appendix.F. For the exact same parameters aside for the initial conditions now being set to $\phi_{21}(0) = \phi_{32}(0) = \pi$ for the π-phase mode, oscillations can be seen. This can be seen in Fig.13. Fig.13a shows that the oscillations initially begin about a non-zero point. Fig.13b indicates a regime of self trapping in the wells.

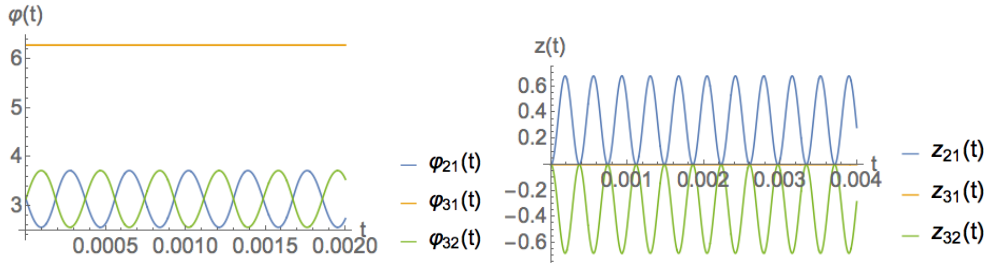

(a) (b)

Figure 13: A plot of $\phi_{21}(t)$, $\phi_{32}(t)$ and $\phi_{31}(t)$ as a function of t in Pane (a). A plot of $z_{21}(t)$ and $z_{32}(t)$ as a function of t in Pane (b) is also produced. The parameters are set to $E_1 = E_2 = E_3 = 0$, $U_1 = U_2 = U_3 = 1$ and $K_{12} = K_{31} = K_{32} = K = 5000$. The Initial conditions were set to $N_1(0) = N_2(0) = N_3(0) = 3000$ and $\phi_{21}(0) = \pi$, $\phi_{21}(0) = \pi$.

B. Varying The Particle Imbalance For A Symmetric Trap

In Fig.14, for $\phi_{21}(0) = \phi_{32}(0) = 0$, the particle imbalance were set to $N_1 = 1000$, $N_2 = 1000$ and $N_3 = 8000$ with all the other parameters the same as the case in Fig13. This setup represents a symmetric triple well where the right well has a much larger number of particles compared to the middle and right well. As can be seen in Fig.14a, the phase difference: $\phi_{32}(t)$ oscillates around zero. In Fig.14b, the particle imbalance: $z_{32}(t)$ oscillates around a non-zero point. This indicates that self trapping has occurred in only the well on the right.

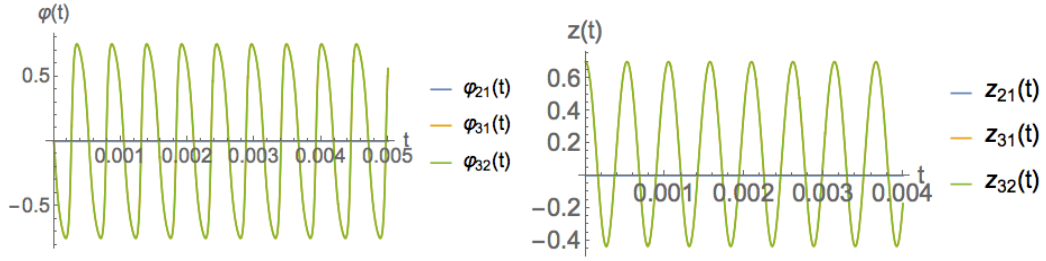

(a) (b)

Figure 14: $\phi(t)$ and $z(t)$ as a function of t such that there is a large number of particles in the right well are produced in Pane (a) and Pane (b) respectively. The parameters are defined within the text.

In Fig.15, the parameters were set to the same value in Fig.14 aside from the initial conditions which were set to $\phi_{21}(0) = \pi$ and $\phi_{32}(0) = \pi$ for a π-phase mode. The plots for both $\phi(0) = 0$ and $\phi(0) = \pi$ are included. In Fig.15a, ϕ_{21} and ϕ_{32} appear to be decreasing as time increases. This indicates that a running-phase mode. This is due to MQST setting in for the left barriers between the middle and left well.

In Fig.16, the number of particles in each well were switched from $N_1 = 1000$, $N_2 = 1000$ and $N_3 = 8000$ to $N_1 = 1000$, $N_2 = 8000$ and $N_3 = 1000$ for $\phi_{21}(0) = 0$ and $\phi_{32}(0) = 0$. In this system, there are oscillations

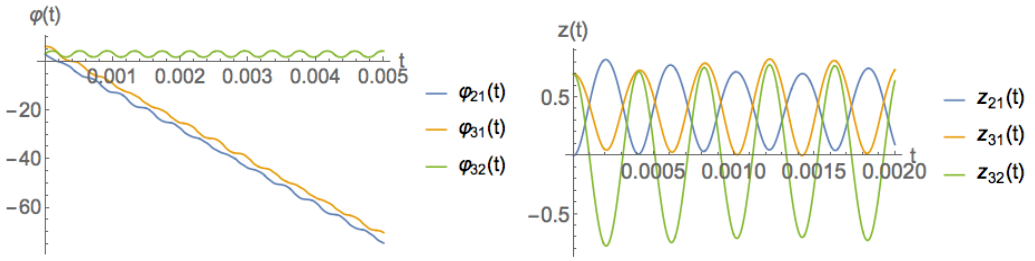

(a) (b)

Figure 15: $\phi(t)$ and $z(t)$ as a function of t are produced in Pane (a) and Pane (b) respectively such that there is a large number of particles in the right for a π-phase mode. The parameters are defined within the text.

however, they now appear to be a lot more an-harmonic. This may be due to the system now becoming more assymetric by starting with a large number of particles in the right well in comparison to the case in Fig.14 where there is a large number of particles in the middle well as the system starts with symmetric initial conditions. Self trapping occurs for both $z_{21}(t)$ and $z_{31}(t)$.

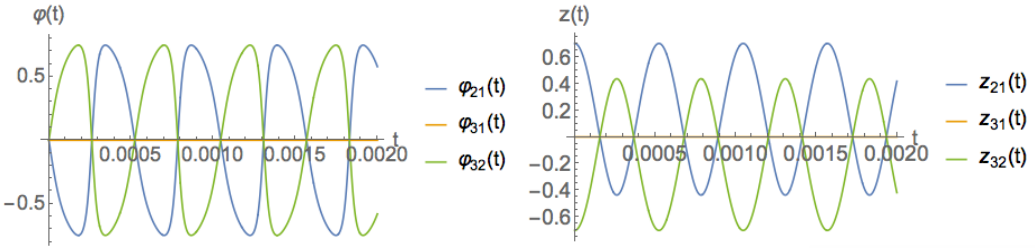

(a) (b)

Figure 16: $\phi(t)$ and $z(t)$ as a function of t for a large number of particles in the middle well are produced in Pane (a) and Pane (b) respectively. The parameters are defined within the text.

In Fig.17, the parameters are identical to what was set in Fig.16b aside from $\phi_{21}(0) = \pi$ and $\phi_{32}(0) = \pi$ for a π-phase mode. For this system, the phase difference oscillates and appears symmetric about a non zero value as time increases. $z(t)$ is symmetric about the time axis for $z_{21}(t)$ and $z_{32}(t)$. Due to this, $z_{31}(t)$ does not oscillate. Varying K_{ab} along with the other parameters will also affect the system. This will be the topic of the next subsection.

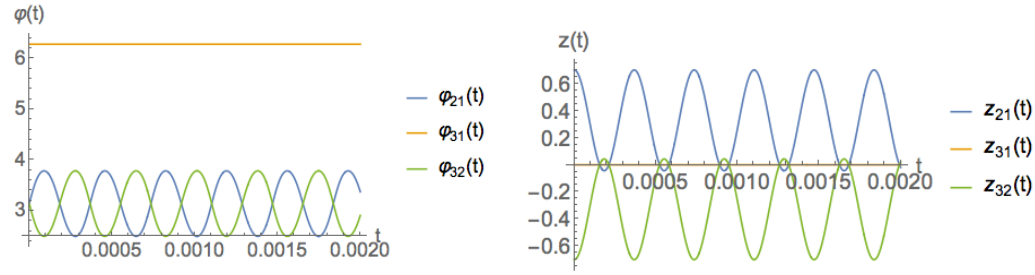

(a) (b)

Figure 17: $\phi(t)$ and $z(t)$ as a function of t for a large number of particles in the middle well are produced in Pane (a) and Pane (b) respectively for a π-phase mode. The parameters are defined within the text.

C. Varying the Coupling Constant For A Symmetric Trap

The coupling constants k_{12}, k_{13} and k_{32} can also be varied whilst beginning with an equal number of particles in each well. In Fig.18, the coupling constant K were set to $K_{12} = 1000$, $K_{23} = 1000$ and $K_{32} = 8000$. The

initial phases were set to $\phi_{21}(0) = 0$, $\phi_{32}(0) = 0$ for Pane (a) and (b) and $\phi_{21}(0) = \pi$, $\phi_{32}(0) = \pi$ for Pane (c) and (d). Fig.18a and Fig.18b represent the system where $\phi_{21}(0) = 0$ and $\phi_{32}(0) = 0$ and Fig.18c and Fig.18d represent the system where $\phi_{21}(0) = \pi$ and $\phi_{32}(0) = \pi$. A running phase appears in both systems however, $\phi(t)$ appears to oscillate over a larger range of values in comparison to Fig.15.

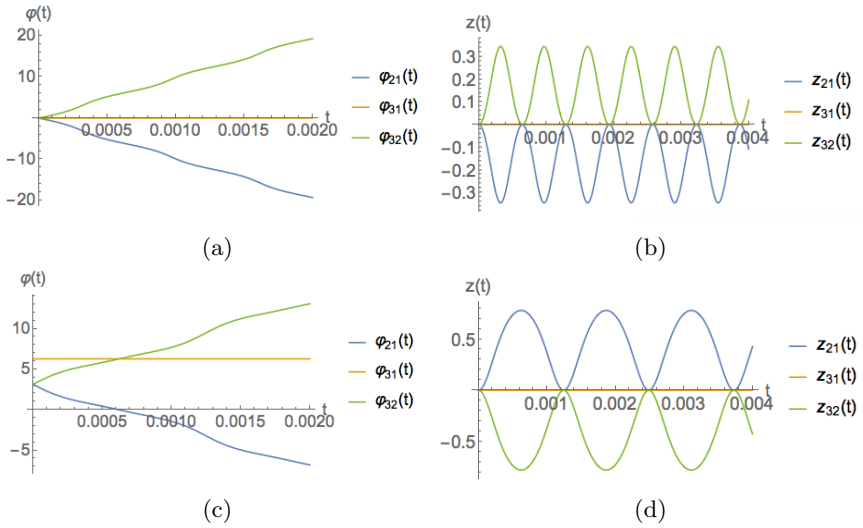

Figure 18: $\phi(t)$ and $z(t)$ as a function of t for a large coupling constant between the middle and right well. The parameters for each Pane are defined within the text.

D. The Asymmetric Triple Well

The parameters E_1, E_2 and E_3 can be changed to increase the energy gap of the three wells. This was investigated by using the same set up to the simplest case mentioned in Sec.IVA. aside from setting the energy parameters now being set to $E_1 = 0$, $E_2 = 1$ and $E_3 = 0$. This system is plotted in Fig.19. $\phi_{21}(t)$ and $\phi_{32}(t)$ oscillate symmetrically about a zero point whereas $z_{21}(t)$ and $z_{32}(t)$ oscillated about a non zero point. By changing E_2, the system becomes asymmetric and thus oscillations are observed in this system as opposed to the system defined by Eq.(60-63) for both $z(t)$ and $\phi(t)$.

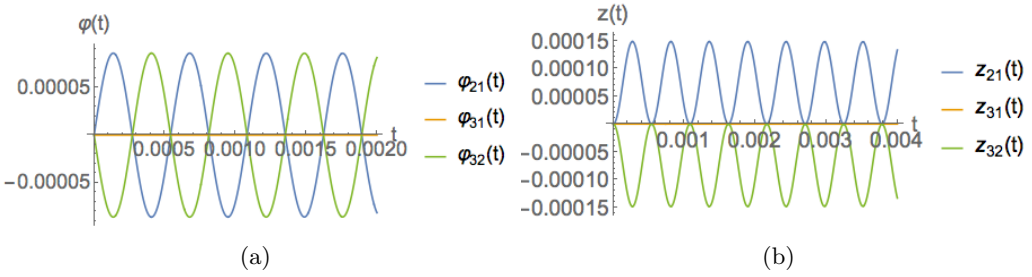

Figure 19: $\phi(t)$ and $z(t)$ as a function of t for an asymmetric trap. The parameters for each Pane are defined within the text.

The energy was then changed to $E_1 = 0$, $E_2 = 0$ and $E_3 = 1$ to see how an energy gap on just the right well would affect the system. This system is plotted in Fig.20. In this system, only ϕ_{32} and z_{32} oscillate. ϕ_{32} oscillated about a zero point and z_{32} oscillated about a non-zero point. This indicates that only particles are exchanged between the middle and right well and none are exchanged between the middle and left well. It is important to note however that both $z(t)$ and $\phi(t)$ oscillate at low values in Fig.19 and Fig.20which indicates that the oscillations are unlikely to be detectable experimentally.

The parameters U_1, U_2 and U_3 along with E_1, E_2 and E_3 were now changed to make the trap slightly more asymmetric. A plot was produced in Fig.21 where the parameters were set to $E_1 = 0$, $E_2 = 0$, $E_3 = 1$, $U_1 = 1$, $U_2 = 10$ and $U_3 = 1$ which is the same system as what was described in Fig.19 aside from $U_2 = 10$ now being set instead of $U_2 = 1$. This makes the system behave differently and produces a running phase mode.

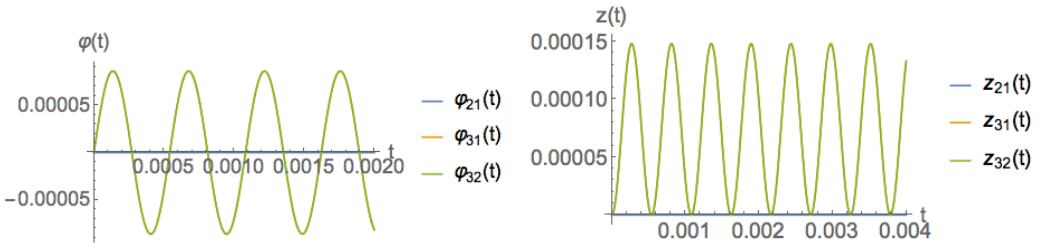

(a) (b)

Figure 20: $\phi(t)$ as a function of t is produced in Pane (a) for both $\phi_{21}(t)$ and $\phi_{32}(t)$. A plot of $z(t)$ as a function of t is produced in Pane (b) for both $z_{21}(t)$ and $z_{32}(t)$. The energy parameters, E_a were set to $E_1 = 0$, $E_2 = 0$ and $E_3 = 1$. The other parameters were set to $U_1 = U_2 = U_3 = 1$ and $K_{12} = K_{31} = K_{32} = K = 5000$. The Initial conditions were set to $N_1(0) = N_2(0) = N_3(0) = 3000$, $\phi_{21}(0) = 0$ and $\phi_{32}(0) = 0$.

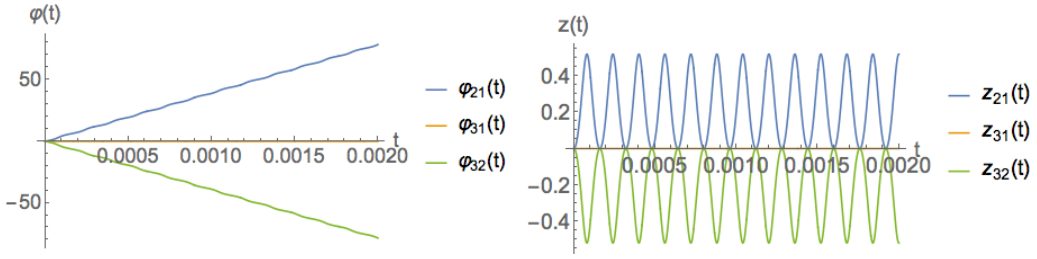

(a) (b)

Figure 21: $\phi(t)$ as a function of t is produced in Pane (a) for both $\phi_{21}(t)$ and $\phi_{32}(t)$. A plot of $z(t)$ as a function of t is produced in Pane (b) for both $z_{21}(t)$ and $z_{32}(t)$. The energy parameters, E_a were set to $E_1 = 0$, $E_2 = 0$ and $E_3 = 1$. The other parameters were set to $U_1 = 1$, $U_2 = 10$ and $U_3 = 1$. The coupling constants were set to $K_{12} = K_{31} = K_{32} = K = 5000$. The Initial conditions were set to $N_1(0) = N_2(0) = N_3(0) = 3000$, $\phi_{21}(0) = 0$ and $\phi_{32}(0) = 0$.

V Summary And Conclusion

The dynamics of two and three weakly coupled BECs were discussed. The dynamics of a boson Josephson junction were also investigated. Rabi−like oscillations were discussed briefly that occur when $\Lambda = 0$ where the oscillation of the particle imbalance is sinusoidal. Increasing Λ was found to make the system an-harmonic. A critical transition was found at $\Lambda = \Lambda_c = 10$ for the symmetric double well trap that was investigated. At this transition, MQST was observed. This occurs when the atomic self-interaction creates a self-maintained population imbalance across the junction. Two types of MQST were found to occur once there is a changeover between the two states occurring at $\Lambda_s = 1/\sqrt{1 - z(0)^2}$. One type of MQST was a running phase mode that occured at $\Lambda = 14.9$. π-oscillations were also observed in which the phase difference across the junction oscillated about π. The dynamics of the symmetric double well were then summarized by using a phase portrait of ϕ and z in Fig.8. An asymmetric trap was then investigated and a running phase mode was observed in Fig.10. Typically neglected terms were also derived and in particular the U_1122 term was included in a calculation to find $z(t)$ and $\phi(t)$. It was found that including the term made the system behave slightly more asymmetric.

Similar types of oscillations were observed in both the double and triple well setup. For example, a running phase oscillation appeared in Fig.10 as well as Fig.18 when the coupling constants where changed. A pendulum analogy was used to give an intuition as to why the system behaved the way it did in Sec.III. The exact same analogy can also be applied to a triple well to gain the same insight as to how each well behaves.

From the data, it can be seen that changing even just one parameter completely changes the overall characteristics of a triple well system. An interesting application of the triple well system is the topic of Ref. [20]. In this paper, the authors showed that the triple well potential structure of a BEC displayed behaviour that was similar to that of a transistor. This is possible as the tunneling of two wells can be controlled by the population of a third well. The system makes it possible to control a large number of atoms using a smaller number of atoms and demonstrated switching and both absolute and differential gain. This is possible as parameters are chosen such that the chemical potential of the middle well is more sensitive to a change in the number of atoms

in the well in comparison to the left and right well. Given more time, an attempt would have been made to create a similar system to see whether it is possible using a semi-classical approach.

The paper also derived the general equations of motion of a BEC in an n-well potential. The results of using a mean field calculation was then compared to a second quantization calculation for a triple well. This would be interesting to investigate further as it would be possible to compare the three models and verify the systems studied in Sec.IV did in-fact give correct results. It would also be possible to investigate when one model may be more appropriate to use and the limitations of each model.

It is also important to note that several problems arose when attempting to plot the triple well. For example, difficulty arose when it was attempted to recast $\dot{N}_1(t)$, $\dot{N}_2(t)$ and $\dot{N}_3(t)$ as $\dot{z}(t)$ using an expression similar to Eq.(87). This meant that $N_1(t)$, $N_2(t)$ and $N_3(t)$ were first solved using a Runge-Kutta method then $z_{21}(t)$, $z_{32}(t)$ and $z_{31}(t)$ were found using Eq.(123). These along with $\phi_{21}(t)$, $\phi_{31}(t)$ and $\phi_{31}(t)$ were then plotted. This was different to the case for the double well discussed in Sec.III where the functions $z(t)$ and $\phi(t)$ were solved directly using a Runge-Kutta method. The timescale also needed to be set to an appropriate value such that it did not take too long to solve the equations computationally.

Overall, the investigation was a success as all the results obtained in Sec.III produced the expected results. This can be verified as Ref. [19] produced similar results for different parameters. Sec.IV largely produced results that appeared to correct as oscillations and a running phase were observed. However, it is not possible to fully justify the results for the triple well being correct as no other literature was found involving the system set up semi-classically.

It is important to note that the derivation of the GPE was in-fact a semi-classical derivation. Despite this, quantum mechanical results such as MQST were obtained in Sec.III. The investigation conducted for the symmetric double-well also agreed with the main literature published on the subject: Ref. [19]. In the triple well case however, the papers such as Ref. [20] and Ref. [21] begin with a purely quantum mechanical setup. Given more time, a purely quantum mechanical framework would have been set up for the triple well case to verify all the results obtained for the triple well.

There are many other systems of BEC that can be investigated, two of which have been mentioned here. They are suitable points of continuation of this report that would have been investigated if not for time constraints.

Transistor like behaviour of a BEC discussed in Ref. [20] was of particular interest as it could have a huge range of applications in research, precision measurements and integrated atom optics.

Super-fluidity is also an interesting consequence of Bose-Einstein condensation. A property that is exhibited by super-fluids is the occurrence of quantum vortices. These are useful system that can be used to better understand surface defects and currents in super-fluids. In a dilute Bose-Einstein gas, vortices can be investigated by starting from the GPE. In this system, the kinetic energy leads to a new centrifugal term. This leads to a modified GPE that can then be solved.

References

[1] E. P. Gross, "Structure of a quantized vortex in boson systems," *Il Nuovo Cimento (1955-1965)*, vol. 20, pp. 454–477, May 1961.

[2] L. P. Pitaevsk, "Vortex lines in an imperfect bose gas," *Soviet Physics JETP-USSR*, vol. 13, no. 2, 1961.

[3] S. N. Bose, "Plancks gesetz und lichtquantenhypothese," *Zeitschrift für Physik*, vol. 26, pp. 178–181, Dec 1924.

[4] F. London, "On the bose-einstein condensation," *Phys. Rev.*, vol. 54, pp. 947–954, Dec 1938.

[5] L. Tisza, "Transport Phenomena in Helium II," *Nature*, vol. 141, p. 913, May 1938.

[6] K. B. Davis, M. O. Mewes, M. R. Andrews, N. J. van Druten, D. S. Durfee, D. M. Kurn, and W. Ketterle, "Bose-einstein condensation in a gas of sodium atoms," *Phys. Rev. Lett.*, vol. 75, pp. 3969–3973, Nov 1995.

[7] M. H. Anderson, J. R. Ensher, M. R. Matthews, C. E. Wieman, and E. A. Cornell, "Observation of bose-einstein condensation in a dilute atomic vapor," *Science*, vol. 269, no. 5221, pp. 198–201, 1995.

[8] B. Josephson, "Possible new effects in superconductive tunnelling," *Physics Letters*, vol. 1, no. 7, pp. 251 – 253, 1962.

[9] F. Dalfovo, S. Giorgini, L. P. Pitaevskii, and S. Stringari, "Theory of bose-einstein condensation in trapped gases," *Rev. Mod. Phys.*, vol. 71, pp. 463–512, Apr 1999.

[10] N. Bogoliubov, "On the theory of superfluidity," *J. Phys*, vol. 11, no. 1, p. 23, 1947.

[11] M. Edwards and K. Burnett, "Numerical solution of the nonlinear schrödinger equation for small samples of trapped neutral atoms," *Phys. Rev. A*, vol. 51, pp. 1382–1386, Feb 1995.

[12] P. A. Ruprecht, M. J. Holland, K. Burnett, and M. Edwards, "Time-dependent solution of the nonlinear schrödinger equation for bose-condensed trapped neutral atoms," *Phys. Rev. A*, vol. 51, pp. 4704–4711, Jun 1995.

[13] F. Dalfovo and S. Stringari, "Bosons in anisotropic traps: Ground state and vortices," *Phys. Rev. A*, vol. 53, pp. 2477–2485, Apr 1996.

[14] R. J. Dodd, M. Edwards, C. J. Williams, C. W. Clark, M. J. Holland, P. A. Ruprecht, and K. Burnett, "Role of attractive interactions on bose-einstein condensation," *Phys. Rev. A*, vol. 54, pp. 661–664, Jul 1996.

[15] M. Holland and J. Cooper, "Expansion of a bose-einstein condensate in a harmonic potential," *Phys. Rev. A*, vol. 53, pp. R1954–R1957, Apr 1996.

[16] T. Schumm, *Bose-Einstein condensates in magnetic double well potentials.* PhD thesis, University of Paris Sud/University of Heidelberg, 2005.

[17] C. Sabín, P. Barberis-Blostein, and I. Fuentes, "Analytical solution of a double-well bose-einstein condensate," *arXiv preprint arXiv:1406.4984*, 2014.

[18] S. Raghavan, A. Smerzi, S. Fantoni, and S. Shenoy, "Coherent oscillations between two weakly coupled bose-einstein condensates: Josephson effects, π oscillations, and macroscopic quantum self-trapping," *Physical Review A*, vol. 59, no. 1, p. 620, 1999.

[19] A. Smerzi, S. Fantoni, S. Giovanazzi, and S. R. Shenoy, "Quantum coherent atomic tunneling between two trapped bose-einstein condensates," *Phys. Rev. Lett.*, vol. 79, pp. 4950–4953, Dec 1997.

[20] J. A. Stickney, D. Z. Anderson, and A. A. Zozulya, "Transistor-like behavior of a bose-einstein condensate in a triple well potential," *Phys. Rev. A*, vol. 75, 01 2007.

[21] T. F. Viscondi and K. Furuya, "Dynamics of a bose-einstein condensate in a symmetric triple-well trap," *Journal of Physics A: Mathematical and Theoretical*, vol. 44, no. 17, p. 175301, 2011.

A Deriving the Time Dependence of The many body Hamiltonian

The many body Hamiltonian (1) written as

$$\hat{H} = \int d\mathbf{r}\, \hat{\Psi}^\dagger(\mathbf{r}) \Big[-\frac{\hbar^2}{2m}\nabla^2 + V_{\text{ext}}(\mathbf{r}) \Big] \hat{\Psi}(\mathbf{r}) + \frac{1}{2}\int d\mathbf{r} d\mathbf{r}'\, \hat{\Psi}^\dagger(\mathbf{r})\, \hat{\Psi}^\dagger(\mathbf{r}') \mathbf{V}(\mathbf{r}-\mathbf{r}')\, \hat{\Psi}(\mathbf{r}')\, \hat{\Psi}(\mathbf{r}), \tag{64}$$

is a suitable stating point for the derivation. The time dependent Schrodinger equation gives

$$i\hbar \frac{\partial}{\partial t}\hat{\Psi}(\mathbf{r},t) = [\hat{\Psi}, \hat{H}] = \hat{\Psi}\hat{H} - \hat{H}\hat{\Psi} \tag{65}$$

where $\hat{\Psi} = \hat{\Psi}(\mathbf{r}'', t)$. Expanding this out fully gives

$$\begin{aligned}[\hat{\Psi}, \hat{H}] = \Psi(\mathbf{r}'', t)\Big[\int d\mathbf{r} \Psi^\dagger(\mathbf{r})[...]\Psi(\mathbf{r}) + \frac{1}{2}\int d\mathbf{r} d\mathbf{r}' \Psi^\dagger(\mathbf{r})\Psi^\dagger(\mathbf{r}')\mathbf{V}(\mathbf{r}-\mathbf{r}')\Psi(\mathbf{r})\Psi(\mathbf{r}')\Big] - \\ \Big[\int d\mathbf{r} \Psi^\dagger(\mathbf{r})[...]\Psi(\mathbf{r}) + \frac{1}{2}\int d\mathbf{r} d\mathbf{r}' \Psi^\dagger(\mathbf{r})\Psi^\dagger(\mathbf{r}')\mathbf{V}(\mathbf{r}-\mathbf{r}')\Psi(\mathbf{r})\Psi(\mathbf{r}')\Big]\Psi(\mathbf{r}'', t),\end{aligned} \tag{66}$$

where $[...] = -\frac{\hbar^2}{2m}\nabla^2 + V_{\text{ext}}(\mathbf{r})$. With further simplification,

$$\begin{aligned}[\hat{\Psi}, \hat{H}] = \int d\mathbf{r} \Psi(\mathbf{r}'')\Psi^\dagger(\mathbf{r})[...]\Psi(\mathbf{r}) - \int d\mathbf{r}\Psi^\dagger(\mathbf{r})[...]\Psi(\mathbf{r})\Psi(\mathbf{r}'') + \\ \frac{1}{2}\int d\mathbf{r} d\mathbf{r}' \Psi(\mathbf{r}'')\Psi^\dagger(\mathbf{r})\Psi^\dagger(\mathbf{r}')\mathbf{V}(\mathbf{r}-\mathbf{r}')\Psi(\mathbf{r})\Psi(\mathbf{r}') - \frac{1}{2}\int d\mathbf{r} d\mathbf{r}' \Psi^\dagger(\mathbf{r})\Psi^\dagger(\mathbf{r}')\mathbf{V}(\mathbf{r}-\mathbf{r}')\Psi(\mathbf{r})\Psi(\mathbf{r}')\Psi(\mathbf{r}'', t).\end{aligned} \tag{67}$$

Using the Dirac delta function given by:

$$\int d\mathbf{r}' \delta(\mathbf{r}-\mathbf{r}') f(\mathbf{r}') = f(\mathbf{r}), \tag{68}$$

the first two terms of Eq.(67) can be re-written as

$$\int d\mathbf{r}' \big[\Psi(\mathbf{r}''), \Psi^\dagger(\mathbf{r})\big] \Big[-\frac{\hbar^2}{2m}\nabla^2 + V_{\text{ext}}(\mathbf{r}) \Big] \Psi(\mathbf{r}), \tag{69}$$

and the final two terms can be re-written as

$$\int d\mathbf{r} d\mathbf{r}' \big[\Psi(\mathbf{r}''), \Psi^\dagger(\mathbf{r})\big] \Psi^\dagger(\mathbf{r}')\mathbf{V}(\mathbf{r}-\mathbf{r}')\Psi(\mathbf{r})\Psi(\mathbf{r}'). \tag{70}$$

Using the Bose commutation relations given by

$$\big[\Psi_1^\dagger(\mathbf{r}), \Psi_2^\dagger(\mathbf{r}')\big] = 0, \tag{71}$$

$$\big[\Psi_1(\mathbf{r}), \Psi_1^\dagger(\mathbf{r}')\big] = \delta(\mathbf{r}-\mathbf{r}'), \tag{72}$$

the two terms can be added to give the final result:

$$i\hbar \frac{\partial}{\partial t}\hat{\Psi}(\mathbf{r},t) = [\hat{\Psi}, \hat{H}] = \Big[-\frac{\hbar^2}{2m}\nabla^2 + V_{\text{ext}}(\mathbf{r}) + \int d\mathbf{r}' \hat{\Psi}^\dagger(\mathbf{r}', t)\mathbf{V}(\mathbf{r}-\mathbf{r}')\hat{\Psi}(\mathbf{r}', t)\Big]\hat{\Psi}(\mathbf{r}'', t). \tag{73}$$

The operator $\hat{\Psi}$ is then replaced with the field operator Φ. In a dilute cold gas as the case with a Bose Einstein , only binary collisions occur at low energy which are only characterized by the parameter of the s-scattering length which is independent of the two-body potential. Because of this, one can replace $\mathbf{V}(\mathbf{r}-\mathbf{r}')$ in Eq.(6) with the effective interaction

$$\mathbf{V}(\mathbf{r}-\mathbf{r}') = g\delta(\mathbf{r}-\mathbf{r}') \tag{74}$$

where the δ indicates a dirac delta function and the coupling constant g is related to the scattering length a by

$$g = \frac{4\pi\hbar^2 a}{m}. \tag{75}$$

Thus, Eq.(73) becomes

$$i\hbar \frac{\partial}{\partial t}\Phi(\mathbf{r},t) = \Big(-\frac{\hbar^2}{2m}\nabla^2 + V_{\text{ext}}(\mathbf{r}) + g|\Phi(\mathbf{r},t)|^2 \Big)\Phi(\mathbf{r},t), \tag{76}$$

which is known as the Gross-Pitaevskii equation (GPE).

B Finding the Double Well trap equations of motion

To find the equations of motion for the double well trap, one starts with Eq.(17-18) defined as:

$$i\hbar\frac{\partial}{\partial t}\psi_1 = (E_1^0 + U_1N_1)\psi_1 - K\psi_2, \tag{77}$$

$$i\hbar\frac{\partial}{\partial t}\psi_2 = (E_2^0 + U_2N_2)\psi_2 - K\psi_1. \tag{78}$$

The condition $U_1 = U_2 = U$ is now imposed. setting $\hbar = 1$ and substituting ψ_1 and ψ_2 both defined in Eq.(16) into Eq.(17) the expression:

$$i\frac{\partial}{\partial t}\sqrt{N_1}e^{i\theta_1} = (E_1^0 + U_1N_1)\sqrt{N_1}e^{i\theta_1} - K\sqrt{N_2}e^{i\theta_2} \tag{79}$$

is obtained. A similar expression can also be obtained for Eq.(18). This derivation will focus on solving Eq.(17) and later produce Eq.(18) when appropriate to do so as the two equations are analogous. Solving the partial derivative on the right hand side of Eq.(79) and dividing through by $e^{i\theta\_1}$, one obtains

$$\frac{-i}{2\sqrt{N_1}}\dot{N}_1 + \sqrt{N_1}\dot{\theta}_1 = (E_1^0 + U_1)\sqrt{N_1} - K\sqrt{N_2}e^{i(\theta_2-\theta_1)}. \tag{80}$$

Using Euler's formula $e^{i\theta} = \cos\theta + i\sin\theta$, the real and imaginary part of Eq.(80) can be equated giving the two equations

$$\frac{1}{2\sqrt{N_1}}\dot{N}_1 = K\sqrt{N_2}\sin(\theta_2 - \theta_1), \tag{81}$$

$$\sqrt{N_1}\dot{\theta}_1 = (E_1^0 + UN_1)\sqrt{N_1} - K\sqrt{N_2}\cos(\theta_2 - \theta_1). \tag{82}$$

Eq.(81) and Eq.(82) can be re-written with $\dot{N}_1$ and $\dot{\theta}_1$ on the left hand side of the two equations respectively. Using the equality, Eq.(22), given as $\phi = \theta_2 - \theta_1$ we arrive to the equations:

$$\dot{N}_1 = 2K\sqrt{N_1N_2}\sin(\phi), \tag{83}$$

$$\dot{\theta}_1 = E_1 + UN_1 - K\sqrt{\frac{N_2}{N_1}}. \tag{84}$$

The analogous equations for $\dot{N}_2$ and $\dot{\theta}_2$ are written as

$$\dot{N}_2 = 2K\sqrt{N_1N_2}\sin(-\phi), \tag{85}$$

$$\dot{\theta}_2 = E_2 + UN_2 - K\sqrt{\frac{N_1}{N_2}}. \tag{86}$$

Using the result

$$\sqrt{N_1N_2} = \frac{1}{2}N_T\sqrt{1-z^2}, \tag{87}$$

as well as $E_2 - E_1 = \Delta E$, Eq.(83-86) can be re-written to give

$$\dot{z}(t) = \frac{\dot{N}_2(t) - \dot{N}_1(t)}{N_T} = 2K\sqrt{1-z^2(t)}\sin\phi(t), \tag{88}$$

$$\dot{\phi}(t) = \dot{\theta}_2(t) - \dot{\theta}_1(t) = \Delta E + UN_T - 2K\cos\phi(t)\left(\sqrt{\frac{N_1}{N_2}} - \sqrt{\frac{N_2}{N_1}}\right). \tag{89}$$

Re-writing Eq.(88-89) in terms of dimensionless time defined as ($t \to t/2K$ and defining the coupling constant as $\Lambda = UN_T/4K$, one finally arrives at the equations of motion defined as:

$$\dot{z}(t) = -\sqrt{1-z^2(t)}\sin\phi(t), \tag{90}$$

$$\dot{\phi}(t) = \Delta E + \Lambda z(t) + \frac{z(t)}{\sqrt{1-z^2(t)}}\cos\phi(t). \tag{91}$$

C Derivation of the extra terms in the coupled differential equations

In this section, Eq.(17-18) will be derived with inclusion of damping and finite temperature effects. This is done by substituting in the ansatz

$$\Psi(\mathbf{r},t) = \psi_1(t)\phi_1(\mathbf{r}) + \psi_2(t)\phi_2(\mathbf{r}) \tag{92}$$

into Eq.(76) otherwise known as the GPE. This gives the result:

$$\begin{aligned} i\hbar\frac{\partial}{\partial t}\Big(\psi_1(t)\phi_1(\mathbf{r}) + \psi_2(t)\phi_2(\mathbf{r})\Big) = -\frac{\hbar^2}{2m}\nabla^2\Big(\psi_1(t)\phi_1(\mathbf{r}) + \psi_2(t)\phi_2(\mathbf{r})\Big) + V_{\text{ext}}(\mathbf{r})\Big(\psi_1(t)\phi_1(\mathbf{r}) + \psi_2(t)\phi_2(\mathbf{r})\Big) \\ +g|\psi_1(t)\phi_1(\mathbf{r}) + \psi_2(t)\phi_2(\mathbf{r})|^2\Big(\psi_1(t)\phi_1(\mathbf{r}) + \psi_2(t)\phi_2(\mathbf{r})\Big). \end{aligned} \tag{93}$$

The equation is then multiplied by $\phi_1^*(t)$, the complex conjugate of $\phi_1(t)$ and integrated over real space. The left hand side of the equation can be simplified as

$$\begin{aligned} i\hbar\int d\mathbf{r}\phi_1^*(t)\frac{\partial}{\partial t}\Big(\psi_1(t)\phi_1(\mathbf{r}) + \psi_2(t)\phi_2(\mathbf{r})\Big) = i\hbar\frac{\partial\psi_1(t)}{\partial t}\int d\mathbf{r}\phi_1^*(t)\phi_1(\mathbf{r}) + i\hbar\frac{\partial\psi_2(t)}{\partial t}\int d\mathbf{r}\phi_1^*(t)\phi_2(\mathbf{r}) = \\ i\hbar\frac{\partial\psi_2(t)}{\partial t}, \end{aligned} \tag{94}$$

which is due to the orthonormality relations $\int d\mathbf{r}\psi_1\psi_1^* = 1$ and $\int d\mathbf{r}\psi_2\psi_1^* = 0$. The first (Kinetic) and second (Potential) term on the left hand side of Eq.(93) simplifies to

$$-\frac{\hbar^2}{2m}\int d\mathbf{r}\psi_1^*(\mathbf{r})\nabla^2\psi_1(\mathbf{r}) + -\frac{\hbar^2}{2m}\int d\mathbf{r}\psi_1^*(\mathbf{r})\nabla^2\psi_2(\mathbf{r}) \tag{95}$$

and

$$\psi_1(\mathbf{t})\int d\mathbf{r}\psi_1^*(\mathbf{r})V_{\text{ext}}(\mathbf{r})\psi_1(\mathbf{r}) + \psi_2(\mathbf{t})\int d\mathbf{r}\psi_1^*(\mathbf{r})V_{\text{ext}}(\mathbf{r})\psi_2(\mathbf{r}) \tag{96}$$

respectively. The modulus in the third (interaction) term can be simplified to

$$|\psi_1(t)|^2|\phi_1(\mathbf{r})|^2 + |\psi_2(t)|^2|\phi_2(\mathbf{r})|^2 + \psi_1^*(t)\psi_2(t)\phi_1^*(\mathbf{r})\phi_2(\mathbf{r}) + \psi_1^*(t)\psi_2^*(t)\phi_1(\mathbf{r})\phi_2^*(\mathbf{r}). \tag{97}$$

This makes it possible to simplify the interaction term to

$$g\int d\mathbf{r}\Big[\psi_1(t)^3|\phi_1(\mathbf{r})|^4 + 3\psi_1(t)\psi_2(t)^2|\phi_1(\mathbf{r})|^2\phi_2(\mathbf{r})^2 + 3\psi_1(t)^2\psi_2(t)|\phi_2(\mathbf{r})|^3\phi_1(\mathbf{r}) + \psi_2(t)^3\phi_1^*(\mathbf{r})\phi_2(\mathbf{r})^3\Big]. \tag{98}$$

Combining all the terms and aranging in terms of factors of $\psi_1(t)$ and $\psi_2(t)$, the following expression is obtained:

$$\begin{aligned} i\hbar\frac{\partial\psi_1(t)}{\partial t} = \psi_1(t)\Big(-\int\frac{\hbar^2}{2m}|\nabla\psi_1(\mathbf{r})|^2 d(\mathbf{r}) + \int V_{\text{ext}}(\mathbf{r})|\phi_1(\mathbf{r})|^2 d(\mathbf{r}) + \psi_1(t)^2\int g|\phi_1(\mathbf{r})|^4 d(\mathbf{r})\Big) \\ +\psi_2(t)\Big(\int d(\mathbf{r})\frac{\hbar^2}{2m}\big(\nabla\phi_1^*(\mathbf{r})\nabla\phi_2(\mathbf{r})\big) + \phi_1^*(\mathbf{r})V_{\text{ext}}(\mathbf{r})\phi_2(\mathbf{r})\Big) \\ +g\Big(\psi_2(t)^3\int d(\mathbf{r})\phi_1^*(\mathbf{r})\phi_2(\mathbf{r})^3 + 3\psi_1(t)\psi_2(t)^2\int d(\mathbf{r})|\psi_1(\mathbf{r})|^2\psi_2(\mathbf{r})^2 + 3\psi_1(t)^2\psi_2(t)\int|\phi_1(\mathbf{r})|^3\phi_2(\mathbf{r})d(\mathbf{r})\Big). \end{aligned} \tag{99}$$

using the previously defined definitions in Eq.(19-21), this can be further simplified to finally give

$$\begin{aligned} i\hbar\frac{\partial\psi_1}{\partial t} = (E_1^0 + U_1N_1)\psi_1 + K\psi_2 + g_0\Big(\psi_2(t)^3\int d2\phi_1^*(\mathbf{r})\phi_2(\mathbf{r})^3 + \\ 3\psi_1(t)\psi_2^2(t)\int d2|\phi_1(\mathbf{r})|^2\phi_2(\mathbf{r})^2 + 3\psi_1(t)^2\psi_2(t)\int d2|\phi_1(\mathbf{r})|^3\phi_2(\mathbf{r})\Big). \end{aligned} \tag{100}$$

D Finding the U_{1122} term

This derivation will focus on solving Eq.(49) as Eq.(50) can be solved analogously. As a symmetric trap is being considered, $\Delta E = 0$ will be set in Eq.(49) and $\hbar$ will be set to zero giving the result

$$i\frac{\partial}{\partial t}\psi_1 = U_{1111}N_1\psi_2 + K\psi_2 + 3U_{1122}\psi_1(t)\psi_2(t)^2. \tag{101}$$

The partial derivative in Eq.(101) is then solved by substituting ψ_1 and ψ_2 defined in Eq.(16) using the same method described in Appendix.B. This gives the expression

$$-i\left[\frac{1}{2\sqrt{N_1}}\dot{N}_1 e^{i\theta_1} + i\sqrt{N_1}\dot{\theta}_1 e^{i\theta_1}\right] = U_{1111}N_1\sqrt{N_1}e^{i\theta_1} + K\sqrt{N_2}e^{i\theta_2} + 3U_{1122}\sqrt{N_1}N_2 e^{i\theta_1}e^{i\theta_2}. \tag{102}$$

Dividing through by $e^{i\theta_1}$ the expression becomes

$$\frac{-i\dot{N}_1}{2\sqrt{N_1}} + \sqrt{N_1}\dot{\phi}_1 = U_{1111}N_1\sqrt{N_1} + K\sqrt{N_2}e^{i\theta_2-\theta_1} + 3U_{1122}\sqrt{N_1}N_2 e^{2i\theta_2}. \tag{103}$$

Using Euler's formula, the real and imaginary part of Eq.(103) are given as

$$\frac{-\dot{N}_1}{2\sqrt{N_1}} = U_{1111}N_1\sqrt{N_1} + K\sqrt{N_2}\sin\phi + 3U_{1122}\sqrt{N_1}N_2\sin(2\theta_2), \tag{104}$$

$$\sqrt{N_1}\dot{\theta}_1 = K\sqrt{N_2}\cos\phi + 3U_{1122}\sqrt{N_1}N_2\cos(2\theta_2). \tag{105}$$

These two expressions can be simplified to

$$\dot{N}_1 = -2K\sqrt{N_1N_2}\sin\phi - 3U_{1122}N_1N_2\sin(2\theta_2), \tag{106}$$

$$\dot{\theta}_1 = U_{1111} + 2K\sqrt{\frac{N_1}{N_2}}\cos\phi + 6U_{1122}N_1N_2\cos(2\theta_2). \tag{107}$$

The analogous equations for $\dot{N}_2$ and $\dot{\theta}_2$ are written as

$$\dot{N}_2 = -2K\sqrt{N_1N_2}\sin(-\phi) - 3U_{2211}N_1N_2\sin(2\theta_1), \tag{108}$$

$$\dot{\theta}_2 = U_{2222} + 2K\sqrt{\frac{N_1}{N_2}}\cos(-\phi) + 6U_{2211}N_1N_2\cos(2\theta_1). \tag{109}$$

Using the result $\sqrt{N_lN_r} = \frac{1}{2}N_T\sqrt{1-z^2}$, Eq.(106-109) can be re-written to give

$$\dot{z}(t) = \frac{\dot{N}_2(t) - \dot{N}_1(t)}{N_T} = \frac{4K\sqrt{N_1N_2}}{N_T}\sin\phi + 3U_{1122}N_1N_2\big(\sin(2\theta_1 - \sin(2\theta_2), \tag{110}$$

$$\dot{\phi}(t) = \frac{\dot{N}_2(t) - \dot{N}_2(t)}{N_T} = U_{1111}N_1 - U_{2222}N_2 + 2K\left(\sqrt{\frac{N_l}{N_r}} - \sqrt{\frac{N_r}{N_l}}\right)\cos\phi + 6U_{1122}N_1N_2\big(\cos(2\theta_1) - \cos(2\theta_2)\big). \tag{111}$$

Using the appropriate trigonometric identities, the equations of motion can be expressed as

$$\dot{z}(t) = \sqrt{1-z^2}\sin\phi - 6U_{1122}N_1N_2\cos(2\theta_1 - \phi)\sin\phi, \tag{112}$$

$$\dot{\phi}(t) = (N_1U_{1111} - N_2U_{2222}) - \frac{z}{\sqrt{1-z^2}}\cos\phi + 12U_{1122}N_1N_2\cos\left(\frac{2\theta_1 - \phi}{2}\right)\sin\phi. \tag{113}$$

E Finding The Equations Of Motion For The Triple Well Bose-Einstein Condensate

Once the ansatz, Eq.53, is substituted into Eq.(76), the only interaction term that is considered is the term defined as

$$g\int d\mathbf{r}|\psi_1|^4. \tag{114}$$

Following the same method conducted in Appendix.C, one arrives at the equation

$$i\hbar\frac{\partial\psi_1}{\partial t} = \psi_1(t)(E_1+U_1) + K_{12}\psi_2(t) + K_{13}\psi_3(t), \tag{115}$$

where E_1 is defined by Eq.(19) and U_1 is defined by Eq.(20). The coupling energy K has a new definition as the three wells are coupled rather than two. It is defined as

$$K_{ab} = \int d\mathbf{r}\frac{-\hbar^2}{2m}\nabla\phi_a(\mathbf{r})\nabla\phi_b(\mathbf{r}) + \int d\mathbf{r}\phi_a(\mathbf{r})V_{\text{ext}}\phi_b(\mathbf{r}). \tag{116}$$

The other two coupled equations can be solved analogously. The three coupled are defined as

$$i\hbar\frac{\partial\psi_1}{\partial t} = \psi_1(t)(E_1+U_1) + K_{12}\psi_2(t) + K_{13}\psi_3(t), \tag{117}$$

$$i\hbar\frac{\partial\psi_2}{\partial t} = \psi_2(t)(E_2+U_2) + K_{21}\psi_1(t) + K_{23}\psi_3(t), \tag{118}$$

$$i\hbar\frac{\partial\psi_3}{\partial t} = \psi_3(t)(E_3+U_3) + K_{31}\psi_1(t) + K_{32}\psi_2(t). \tag{119}$$

These three equations can be split into real and imaginary parts following the same method conducted in Appendix.D. This leads to two expressions defined as:

$$\dot{N}_1 = -2K_{12}\sqrt{N_1N_2}\sin(\theta_2-\theta_1) - 2K_{13}\sqrt{N_1N_3}\sin(\theta_3-\theta_1), \tag{120}$$

$$\dot{\theta}_1 = E_1 + U_1N_1 + K_{12}\sqrt{\frac{N_2}{N_1}}\cos(\theta_2-\theta_1) + K_{13}\sqrt{\frac{N_3}{N_1}}\cos(\theta_3-\theta_1). \tag{121}$$

Analogous equations for $\dot{N}_2$, $\dot{N}_3$, $\dot{\theta}_2$ and $\dot{\theta}_3$ can also be derived. These six equations lead to three equations for the phase difference and population imbalance. They are defined as

$$\phi_{21}(t) = \theta_2(t)-\theta_1(t), \quad \phi_{31}(t) = \theta_3(t)-\theta_1(t), \quad \phi_{32}(t) = \theta_3(t)-\theta_2(t) \tag{122}$$

and

$$z_{21}(t) = \frac{N_2(t)-N_1(t)}{N_1(t)+N_2(t)+N_3(t)}, \quad z_{31}(t) = \frac{N_3(t)-N_1(t)}{N_1(t)+N_2(t)+N_3(t)}, \quad z_{32}(t) = \frac{N_3(t)-N_2(t)}{N_1(t)+N_2(t)+N_3(t)}. \tag{123}$$

Without any simplifications, the three phase differences are defined as

$$\dot{\phi}_{21}(t) = (E_2-E_1)+(U_2N_2-U_1N_1)+K_{12}\left(\sqrt{\frac{N_1}{N_2}}-\sqrt{\frac{N_2}{N_1}}\right)\cos\phi_{21}-K_{13}\sqrt{\frac{N_3}{N_1}}\cos\phi_{31}+K_{32}\sqrt{\frac{N_3}{N_2}}\cos\phi_{32}, \tag{124}$$

$$\dot{\phi}_{31}(t) = (E_3-E_1)+(U_3N_3-U_1N_1)+K_{13}\left(\sqrt{\frac{N_1}{N_3}}-\sqrt{\frac{N_3}{N_1}}\right)\cos\phi_{31}-K_{21}\sqrt{\frac{N_2}{N_1}}\cos\phi_{21}+K_{32}\sqrt{\frac{N_3}{N_2}}\cos\phi_{32}, \tag{125}$$

$$\dot{\phi}_{32}(t) = (E_3-E_2)+(U_3N_3-U_2N_2)+K_{32}\left(\sqrt{\frac{N_2}{N_3}}-\sqrt{\frac{N_3}{N_2}}\right)\cos\phi_{32}-K_{21}\sqrt{\frac{N_1}{N_2}}\cos\phi_{21}+K_{31}\sqrt{\frac{N_1}{N_3}}\cos\phi_{31}. \tag{126}$$

The three expression for the population imbalance are given as

$$\dot{z}_{21}(t) = \frac{4K_{12}\sqrt{N_1N_2}\sin\phi_{21} - 2K_{23}\sqrt{N_2N_3}\sin\phi_{32} + 2K_{13}\sqrt{N_1N_3}\sin\phi_{31}}{N_1+N_2+N_3}, \tag{127}$$

$$\dot{z}_{31}(t) = \frac{4K_{13}\sqrt{N_1N_3}\sin\phi_{31} - 2K_{23}\sqrt{N_2N_3}\sin\phi_{32} + 2K_{12}\sqrt{N_1N_2}\sin\phi_{21}}{N_1+N_2+N_3}, \tag{128}$$

$$\dot{z}_{32}(t) = \frac{4K_{32}\sqrt{N_3N_2}\sin\phi_{32} - 2K_{13}\sqrt{N_1N_3}\sin\phi_{31} + 2K_{12}\sqrt{N_1N_2}\sin\phi_{21}}{N_1+N_2+N_3}. \tag{129}$$

Eq.(124-129) are the equations that will be solved and discussed in the main section using a Runge-Kutta method.

F Example of the Mathematica code used to solve the coupled partial differential equations

```
E1 = 0;
E2 = 0;
E3 = 0;
U1 = 1;
U2 = 1;
U3 = 1;
k12 = k21 = 5000;
k23 = k32 = 3000;
k13 = k31 = 1000;
icp = Pi;
icpN1 = 5000;
icpN2 = 2000;
icpN3 = 1000;

genp21eq =
  Simplify[p21'[t] == (E2 - E1) + ((U2 * N2[t]) - (U1 * N1[t])) + k12 * ((Sqrt[N1[t] / N2[t]] - Sqrt[N2[t] / N1[t]])) Cos[p21[t]] -
     ((k13 * Sqrt[N3[t] / N1[t]]) Cos[p21[t] + p32[t]]) + ((k23 * Sqrt[N3[t] / N2[t]]) Cos[p32[t]])];
genp32eq =
  Simplify[p32'[t] == (E3 - E2) + ((U3 * N3[t]) - (U2 * N2[t])) + k23 * ((Sqrt[N2[t] / N3[t]] - Sqrt[N3[t] / N2[t]])) Cos[p32[t]] -
     ((k12 * Sqrt[N1[t] / N2[t]]) Cos[p21[t]]) + ((k13 * Sqrt[N1[t] / N3[t]]) Cos[p21[t] + p32[t]])];

genN1eq =
  Simplify[N1'[t] == (-2 * k12 * Sqrt[N1[t] * N2[t]] * Sin[p21[t]]) - (2 * k13 * Sqrt[N1[t] * N3[t]] * Sin[p21[t] + p32[t]])];
genN2eq = Simplify[N2'[t] == (+2 * k12 * Sqrt[N1[t] * N2[t]] * Sin[p21[t]]) - (2 * k23 * Sqrt[N2[t] * N3[t]] * Sin[p32[t]])];
genN3eq = Simplify[N3'[t] == (+2 * k31 * Sqrt[N1[t] * N3[t]] * Sin[p21[t] + p32[t]]) + (2 * k32 * Sqrt[N3[t] * N2[t]] * Sin[p32[t]])];

solp21 = NDSolve[{genp21eq, genp32eq, genN1eq, genN2eq, genN3eq, N1[0] == icpN1, N2[0] == icpN2, N3[0] == icpN3,
    p21[0] == icp, p32[0] == icp}, p21, {t, 0, 0.1}];
solp32 = NDSolve[{genp21eq, genp32eq, genN1eq, genN2eq, genN3eq, N1[0] == icpN1, N2[0] == icpN2, N3[0] == icpN3,
    p21[0] == icp, p32[0] == icp}, p32, {t, 0, 0.1}];

solN1 = NDSolve[{genp21eq, genp32eq, genN1eq, genN2eq, genN3eq, N1[0] == icpN1, N2[0] == icpN2, N3[0] == icpN3,
    p21[0] == icp, p32[0] == icp}, N1, {t, 0, 0.1}];
solN2 = NDSolve[{genp21eq, genp32eq, genN1eq, genN2eq, genN3eq, N1[0] == icpN1, N2[0] == icpN2, N3[0] == icpN3,
    p21[0] == icp, p32[0] == icp}, N2, {t, 0, 0.1}];
solN3 = NDSolve[{genp21eq, genp32eq, genN1eq, genN2eq, genN3eq, N1[0] == icpN1, N2[0] == icpN2, N3[0] == icpN3,
    p21[0] == icp, p32[0] == icp}, N3, {t, 0, 0.1}];

p21andp32plot = Plot[Evaluate[{
     p21[t] /. solp21, ((p21[t] /. solp21) + (p32[t] /. solp32)), p32[t] /. solp32}],
   {t, 0, 0.01}];

z21andz32plot =  Plot[Evaluate[{
     ((N2[t] /. solN2) - (N1[t] /. solN1)) / ((N1[t] /. solN1) + (N2[t] /. solN2) + (N3[t] /. solN3)),
     ((N3[t] /. solN3) - (N1[t] /. solN1)) / ((N1[t] /. solN1) + (N2[t] /. solN2) + (N3[t] /. solN3)),
     ((N3[t] /. solN3) - (N2[t] /. solN2)) / ((N1[t] /. solN1) + (N2[t] /. solN2) + (N3[t] /. solN3))
    }], {t, 0, 0.01}];
```

Figure 22: Eq.(124-129) were solved by solving Eq.(127) and Eq.(129) as well as Eq.(120) and the similar equations $\dot{N}_2(t)$ and $\dot{N}_3(t)$ simultaneously. Eq.(123) was then used to find $Z_{21}(t)$, $Z_{32}(t)$ and $Z_{31}(t)$. These results were then plotted using the Plot keyword.